Improving mass redistribution estimates by modeling ocean bottom pressure uncertainties

S.-E. Brunnabend[1], R. Rietbroek[2], R. Timmermann[1], J. Schröter[1], J. Kusche[2]

S.-E. Brunnabend, Alfred-Wegener-Institute (AWI), Bussestr. 24, D-27570 Bremerhaven, Germany, (Sandra-Esther.Brunnabend@awi.de)

R. Rietbroek, Institute of Geodesy and Geo-information, University of Bonn, Nussallee 17, D-53115 Bonn, Germany, (roelof@geod.uni-bonn.de)

J. Schröter, Alfred-Wegener-Institute (AWI), Bussestr. 24, D-27570 Bremerhaven, Germany, (Jens.Schroeter@awi.de)

R. Timmermann, Alfred-Wegener-Institute (AWI), Bussestr. 24, D-27570 Bremerhaven, Germany, (Ralph.Timmermann@awi.de)

J. Kusche, Institute of Geodesy and Geo-information, University of Bonn, Nussallee 17, D-53115 Bonn, Germany, (kusche@geod.uni-bonn.de)

[1]Alfred-Wegener-Institute, Bremerhaven, Germany

[2]Institute for Geodesy and Geo-information, Bonn, Germany

Abstract. Weekly ocean bottom pressure anomalies (OBP) are modeled using the finite element sea-ice ocean model (FESOM). The model's OBP error, mostly unknown so far, is assessed by comparing two model simulations, each forced by different atmospheric forcing datasets. The mean estimated error of modeled OBP is found to be 0.04 m per $1.5^o \times 1.5^o$ grid cell. The error varies strongly from 0.003 m in the equatorial region to 0.31 m in the Weddell and Ross Seas. We believe that the spatial variations of the errors are an important improvement over previous error models. The new error estimates are implemented in a joint inversion of GRACE gravity measurements, GPS site displacements and modeled OBP, resulting in a larger overall OBP weight in the inversion, most notably in the Polar Regions. Additionally, the inversion provides a global mass correction term to adjust the ocean mass budget of the model. The estimated term is used to correct the model's fresh water balance, making it consistent with GRACE and GPS on seasonal and longer time scales. All model results, weekly GRACE estimates and the inverse solutions are compared with measurements from in-situ bottom pressure recorders. The newly estimated error-model of the combination solution results in higher correlations than the previously used constant error-model of the combination solution.

1. Introduction

Ocean mass variations have been measured only on regional scales before satellite measurements have become available (e.g. from the Gravity Recovery and Climate Experiment (GRACE)). Only since the launch of the GRACE satellites in 2002 has it been possible to measure global ocean mass variations directly on a global scale (*Tapley et al.* [2004]; *Bingham and Hughes* [2006]; *Dobslaw and Thomas* [2007]; *Ponte et al.* [2007]; *Chambers and Wahr* [2009]; *Macrander et al.* [2010] and many others). Geopotential Stokes coefficients are provided by the three centers that form the GRACE science data system (GFZ, CSR, and JPL) and a few others (Bonn University, GRGS Toulouse, and TU Delft). These centers use different processing techniques and different temporal resolution, which range from daily to monthly estimates. For most applications, the solutions require additional filtering to suppress (anisotropic) errors. Different filter techniques have been developed, such as the Gauss filter, the pattern filter [*Böning et al.*, 2008], the decorrelation filter [*Kusche*, 2007], or the de-striping filter developed by *Swenson and Wahr* [2006], and later modified by *Chambers* [2006] for oceanographic signals. A drawback of filtering is that it not only reduces the resolution dependent and anisotropic errors [*Thomson et al.*, 2004; *Seo et al.*, 2008; *Chen et al.*, 2009], but also the signal under consideration.

Measurements from ocean bottom pressure recorders (OBPR) have been compared with GRACE solutions and modeled OBP on daily and monthly time scales [*Kanzow et al.*, 2005; *Rietbroek et al.*, 2006; *Park et al.*, 2008; *Böning et al.*, 2008, 2009; *Macrander et al.*, 2010]. GRACE solutions fit reasonably well with in-situ measurements from OBPR in the Polar Regions (with correlations mostly higher than 0.5) [*Macrander et al.*, 2010].

Park et al. [2008] validated GRACE estimates with in-situ OBP measurements in the Kuroshio Extension and showed that GRACE can provide high-quality OBP variations on monthly time scales in this region. *Morison et al.* [2007] found high correlations between in-situ bottom pressure measurements and GRACE estimates at two locations in the Arctic Ocean near the North Pole. In many other regions the correlation between GRACE and OBPR measurements is generally weaker. A particular problem is geocenter motion, which cannot be measured by GRACE as the two satellites orbit the center of mass of the total Earth system. On the other hand the total ocean mass and thus OBP is sensitive to geocenter movements as it is measured relative to the Earth's crust. This issue has been already addressed in earlier GRACE related research [*Chambers, et al.*, 2004], and a model-aided geocenter motion correction has later been constructed by *Swenson et al.* [2008].

Wu et al. [2006] and more recently *Wu et al.* [2010] estimated global surface mass distributions up to order and degree 50 on monthly time scales by combining GRACE gravity data with GPS displacements and ocean bottom pressure derived from the Estimating Circulation and Climate of the Ocean (ECCO) model [*Stammer et al.*, 2002]. The ocean circulation model used, had altimetry data assimilated. *Wu et al.* [2006] assumed a spatially uniform error for modeled OBP of 1.7 cm for monthly averaged $1^o \times 1^o$ grid cells. Such an inversion scheme has been investigated by *Jansen et al.* [2009a], which combines GRACE gravity data, GPS site displacements and OBP from the ECCO model to estimate spherical harmonics coefficients up to degree and order 30 on monthly time scales including the geocenter motion. The error of modeled OBP was assumed to be 5 cm, which corresponds to the error of the satellite altimetry measurements that are assimilated to the model. Initial studies have also been made using the Finite Element Sea-ice Ocean Model (FESOM; *Timmermann et al.* [2009]) instead of the ECCO model [*Jansen et al.*, 2009b]. Weekly combinations are constructed up to degree and order 30, which use weekly GPS solutions, weekly modeled OBP, and sub-monthly GRACE solutions. An uncorrelated error of 5 cm per block-averaged grid cell $5^o \times 5^o$ has been assumed for modeled OBP.

GRACE solutions with higher temporal resolution were calculated by *Dahle et al.* [2008], and used in a joint inversion by combining data from GPS, GRACE and FESOM on weekly time scales [*Rietbroek et al.*, 2009]. The FESOM model [*Timmermann et al.*, 2009] provided modeled OBP as pseudo observations to the inversion. The error of modeled OBP from FESOM has been largely unknown and a constant (area weighted) error of 10 cm for a $1.5^o \times 1.5^o$ grid cell was assumed.

In this study we estimate the OBP error of FESOM and assess its impacts on the estimation of ocean mass redistribution from *Rietbroek et al.* [2009]. Note that FESOM is a pure forward model, i.e. no assimilation of measured data like radar altimetry is performed. Among other factors, modeled ocean circulation is highly dependent on the atmospheric conditions. Here, the error of modeled OBP is estimated by comparing two model simulations using different meteorological datasets as forcing. *Ponte et al.* [2007] estimated a spatially varying OBP error for ECCO by comparing two different ECCO model runs. Additionally, they concluded that GRACE data could provide useful large scale information to the ocean model on seasonal time scales. We investigate how the modeling of the OBP error influences the least squares combination of GRACE measurements, GPS site displacements and modeled OBP of *Rietbroek et al.* [2009]. The inversion also provides a mass correction parameter, which is used to optimize the mass balance in the FESOM model. Finally, all results are compared with in-situ bottom pressure measurements from the AWI database [*Macrander et al.*, 2010].

2. Model and Methods

2.1. Finite Element Sea-Ice Ocean Model

The finite element sea-ice ocean model (FESOM; *Timmermann et al.* [2009]) is used to simulate ocean mass variations on weekly time scales. It couples the finite element ocean model (FESIM; *Danilov et al.* [2004, 2005] with a dynamic-thermodynamic sea-ice model (FESIM; *Danilov and Yakovlev* [2003]), which simulates the prognostic variables sea-ice concentration, sea-ice and snow thickness. The FESOM model is a hydrostatic ocean circulation model with spherical geometry, which solves the hydrostatic primitive equations. It applies the Boussinesq approximation that simplifies the continuity equation and models gravity dependent flows where density variations can be neglected. The approximation can be used if vertical velocities are small and density variations have only small impacts on other forces. Applying the Boussinesq approximation results in conservation of volume. To achieve conservation of mass a correction after Greatbatch is applied [*Greatbatch*, 1994; *Böning et al.*, 2008]. This correction is applied locally at every grid point and recovers the steric contribution, which is neglected in the Boussinesq approximation.

The FESOM model uses a triangular grid for spatial discretisation with a resolution of 1.5 degrees at the ocean surface. The nodes of the 26 z-levels are aligned directly under the surface nodes forming a tetrahedral 3D mesh. The nodes of the deepest elements are allowed to deviate from the z-level to follow realistic ocean bottom topography [*Timmer-*

mann et al., 2009]. The model is initialized with temperature and salinity of the World Ocean Atlas (WOA01) and has a free surface, i.e. it is wind and pressure driven. The ocean state is simulated from 1958 to 2002, in order to spin-up the model.

From 2003 to 2008 weekly means are calculated according to the same weekly increments used by the GPS and GRACE products. Ocean bottom pressure can be derived by integrating the simulated density profile of the water column. It is computed as

$$p(\lambda, \phi, t) = \int_{-H}^{0} \rho(\lambda, \phi, t, z)\, g\, dz + \int_{0}^{h(\lambda,\phi,t)} \rho_w\, g\, dz + p_a(\lambda, \phi, t) \qquad (1)$$

where H is ocean depth, h is the sea surface elevation, $\rho_w = 1027\, kg\, m^{-3}$ the reference density of sea water, ρ the in-situ density, $g = 9.806\, m\, s^{-2}$ the gravitational acceleration, p_a the atmospheric sea level pressure; λ is latitude, and ϕ is longitude. OBP anomalies are computed by subtracting the multi-year mean at each grid point, and are converted to equivalent water height by dividing the anomalies by ρ_w and g (Figure 1a and 1b). We constructed a reference simulation by forcing the model with the atmospheric parameters wind at 10 m above the ocean surface, temperature at 2 m above the ocean surface, specific humidity, total cloud cover and sea level pressure from the NCEP/NCAR reanalysis [*Kalnay*, 1996]. The fresh water budget is fed by net precipitation, which is computed from total precipitation and evaporation, also provided by the NCAR/NCEP reanalysis. As the evaporation fields are not directly available in the reanalysis they are computed from latent heat flux. River runoff, introduced into the model, originates from the Land Surface Discharge Model (LSDM; *Dill* [2008]). All fresh water fluxes are added into the model as daily volume fluxes. The mass balance of these source terms is not in equilibrium [*Kalnay*, 1996]. To avoid unrealistic trends in the global ocean mass, we followed the method of *Böning et al.* [2008]. Accordingly, a two year high pass filter eliminates trends in ocean mass on longer time scales. Hence, no long-term trends in modeled ocean mass variations can be investigated using the reference model setup.

2.2. Estimation of modeled ocean bottom pressure error

Up to now, the error of modeled OBP anomalies simulated with FESOM has been largely unknown. Therefore, several investigations have been performed, such as analyzing the influence of spatial discretisation on the model results. A second model simulation with a similar grid, but with a smoother topography, has been calculated. The results show only minor differences probably due to the relative coarse resolution of the model grid.

Errors are mainly introduced into the model results by the atmospheric forcing fields, as they are the major driver of modeled ocean circulation. Additionally, the modeled mass exchange between atmosphere, ocean, and land is determined by the input parameters, directly propagating their uncertainties [*Kalnay*, 1996; *Hagemann et al.*, 2005; *Berrisford*, 2009] into the model results. Since atmospheric forcing is the largest error source in the model results, its uncertainty is estimated by comparing two model runs using different atmospheric forcing fields (incl. precipitation and evaporation) from the weather forecasts centers NCAR/NCEP and ECMWF. Daily mean fields of the NCEP reanalysis are used in the reference model simulation. The alternative simulation is forced by the 6 hourly ERA Interim reanalysis starting from 1989 [*Simmons et al.*, 2006]. Up to 1989, the model is forced with the ERA40 reanalysis [*ECMWF*, 1995; *Uppala et al.*, 2005; *Berrisford*, 2009]. The error of modeled OBP, $\triangle p$, is computed for every week from 2003 to 2008 by calculating the weekly root mean square (RMS) of the difference of daily mean OBP anomalies (Figure 1c and 1d),

$$\triangle p(\lambda, \phi) = \sqrt{\frac{1}{7}\sum_{d=1}^{7}(\bar{p}_N^d(\lambda, \phi) - \bar{p}_E^d(\lambda, \phi))^2} \quad (2)$$

where $\bar{p}_N^d$ are daily mean OBP anomalies modeled with forcing from the NCAR/NCEP reanalysis and $\bar{p}_E^d$ are daily mean OBP anomalies modeled with forcing from ERA-Interim reanalysis.

2.3. Joint Inversion

The error of modeled OBP is used to weigh the model in the joint inversion, which combines modeled OBP from FESOM, GRACE gravity data and GPS site displacements. We estimate global surface loading, geocenter motion, and a mass correction, which can be used to correct fresh water fluxes in the model [*Rietbroek et al.*, 2009]. The weekly inversion is aligned with the GPS week calendar and is calculated for the period 2003 - 2007 (GPS weeks from 1200 to 1459). The independent datasets are combined by weighted least-squares estimation.

The inversion uses weekly GRACE solutions, which are computed with the same processing standards and background models as the monthly GFZ RL04 solutions [*Dahle et al.*, 2008]. Limitations in maximum resolution result from separation of the satellite ground tracks and data availability. Therefore, a ground track analysis has been performed which indicates that optimal solutions are achievable with spherical harmonics coefficients of degree and order up to 30 × 30 [*Dahle et al.*, 2008]. GRACE gravity solutions are used for the period from GPS weeks 1200 to 1459 (January 2002 until December 2007). Only, seven weeks are missing (GPS weeks 1220-1223 and 1253-1255) because of erroneous GRACE level 1b data. For this reason, the inversion has not been performed during those time periods. The error of weekly GRACE estimates (*Flechtner et al.* [2010]; Figure 1e) mostly originates from resolution dependent errors as well as from aliasing.

Aliasing effects describe the errors in the short wavelength signals (high degree spherical harmonic coefficients) and result in striped mass estimates [*Swenson and Wahr*, 2006]. Therefore, filtering is needed, which not only corrects for the stripes but also influences the geophysical signal. In addition, leakage effects occur because land signals are mixed with ocean signals near coast lines. This effect is prevalent in regions of strong variations in land hydrology, like the Amazonas. The weekly GRACE solutions are not filtered before they are used in the inversion. Additional uncertainties are introduced by using external data for postglacial rebound, atmospheric pressure and the geocenter motion when computing ocean mass variations [*Quinn and Ponte*, 2010]. The GRACE solutions used in this study do not include geocenter motion, due to the limited capability of estimation with GRACE. The movement of the geocenter influences the estimation of global ocean mass and thus OBP. To solve this issue, and to increase the correlation of ocean mass variations with OBPR, the joint inversion provides estimates of geocenter motion constrained by GPS site displacements [*Blewitt*, 2003].

Weekly files of Solution Independent Exchange format (SINEX) from globally distributed International Global navigation satellite system Service (IGS) stations are used to process time series of station displacements including their error-covariance matrix. The results are expressed in spherical harmonics of surface loading mass using methods described by *Kusche and Schrama* [2005]. During an extensive preprocessing several stations are removed, e.g. because of discontinuities in time and to avoid time series shorter than 1 year. The remaining number of stations amounts to 150-200 per week. The spatial resolution of this dataset is limited to thousands of kilometers as GPS stations are not evenly distributed over the Earth, i.e. varying density and heterogeneity [*Jansen et al.*, 2009a]. Within the inversion scheme, GPS displacements mainly contribute to the detection of degree 1 deformation, which can be linked to the geocenter motion, and the estimation of long wavelength surface loading.

In the first inversion, an uncorrelated modeled OBP error of 10 cm is assumed for every 1.5×1.5 degree grid cell, which is scaled with 1/cos(latitude), to mitigate the effect of decreasing area at the poles. To investigate how the error of modeled OBP influences the inverse solution, a second inversion is computed where the assumed constant error is replaced by the error estimated from equation 2.

The global mass correction parameter, derived by the inversion, is used to improve the fresh water budget of FESOM. This is needed because modeled global mean ocean mass variations directly result from the input parameters from NCEP (precipitation) and the LSDM model (river runoff). Hence, all uncertainties included in these parameters are directly reflected in the model results. In addition, the high pass filter, applied to the mass budget of the model simulation, induces an incapability to analyze long term trends of modeled global mean mass variations. Within the inversion, the mass correction parameter is defined as a uniform layer, which allows for the estimation of the offset between the modeled mean ocean mass and the GPS and GRACE datasets. Therefore, the modeled global mean ocean mass does not affect the inversion results. It is derived from the GPS measurements and the GRACE estimates. The correction obtained from the inversion can now be again introduced into the model as the scaling factor β, which varies the precipitation by the amount of the mass correction term (eq. 3).

$$\beta = 1 - \frac{\triangle M}{P} \tag{3}$$

where P is global weekly integrated precipitation and $\triangle M$ is the mass correction term. In the model, the precipitation fields are multiplied with β and a subsequent model integration is performed.

3. Results

3.1. Modeled ocean bottom pressure and its error

The modeled weekly variations in OBP (Figure 1a) reach amplitudes up to 0.08 m regionally. For example, the wind driven oscillation in the North Pacific Ocean is clearly visible. Furthermore, strong variability occurs in the Southern Ocean, with strongest signal west of the Drake Passage, where the OBP signal is highly dependent on the bottom topography (Figure 1b). Short term variations occur in the Arctic Ocean, which generally responses uniformly to varying wind and atmospheric pressure fields. Also semi-enclosed seas, like the Mediterranean Sea and the Hudson Bay, show high variability due to their sensitivity to changes in the model configuration. Generally, OBP variations are high in regions of strong ocean currents, such as the Kuroshio, the Antarctic Circumpolar Current, and the Gulf Stream. In other regions in the open ocean, variability of OBP is relatively moderate.

The mean error of modeled OBP, as obtained from the difference between the two model runs, is 0.04 m per $1.5^o \times 1.5^o$ grid cell and varies strongly with location. The weekly error maps show similar geographical patterns, varying in order of magnitude of mm. For example, the error for week 1400 (the first full GPS week in January 2003) ranges between

0.003 m in the open ocean near the equator and 0.31 m in the Weddell and Ross Seas (Figure 1c). An error of about 0.1 m is found in the Southern Ocean west of the Drake Passage, which originates from differences in the wind fields of the atmospheric datasets. The Arctic Ocean also appears to be sensitive to perturbations in forcing fields, which result from the relatively low spatial resolution in north-south direction. Larger errors occur in the Norwegian Sea and near the east coast of Canada, where the model shows some weakness in the ocean circulation.

The RMS of the differences between the model runs indicates higher deviations in the Southern Ocean because of the strong Antarctic Circumpolar Current (Figure 1d). In regions which are not well connected to the open ocean, such as the Mediterranean Sea and the Hudson Bay, the model is also sensitive to small changes in atmospheric conditions.

The regional distribution of the error corresponding to the GRACE estimates [*Flechtner et al.*, 2010] mainly reflects the error due to the aliasing effect, which is strongest in the equatorial region and displays no geographical patterns (Figure 1e). In the polar region the error reduces due to the denser GRACE ground tracks. Note that in most regions the error of modeled OBP is smaller than the error of the GRACE estimates, but modeled OBP anomalies also show less temporal variations compared to ocean mass variations estimated from GRACE (Figure 1f).

Relatively large differences occur among the two model runs in the variations of modeled global mean ocean mass (Figure 2a). This is due to significant differences between precipitation and evaporation estimates from both weather forecasting centers, however, the seasonal cycles are in phase. The amplitude of the simulation using atmospheric parameters from the ERA Interim reanalysis is lower and decreases in 2007. As expected, both time series show similar structures in short-term variations as both atmospheric datasets are optimized for short term forecasting and are, therefore, well defined in its short term variations.

The estimated error of modeled OBP does not include all possible error sources, such as uncertainties in river runoff input fields or uncertainties arising from the numerics in the model. In addition, the model results suffer from the low spatial resolution, i.e. error estimates caused by missing small scale features like eddies are not taken into account. Correlated errors of the atmospheric forcing fields might exist, as they use overlapping input data. Hence, some error in the input data might result in similar errors in the atmospheric forcing fields, which would be canceled out when computing differences between the two FESOM model results. However, as the atmospheric forcing mostly uses the same input data, the differences in the provided forcing fields mostly result from different processing strategies. These differences can be directly related to uncertainties in the atmospheric parameters. Using two model simulations, forced by different atmospheric input, enables the estimation of error maps. These show regional patterns, which can be related to geophysical features. For example, higher errors appear in the Arctic Ocean where modeled ocean circulation might not be trusted, as a small Island is included into the model grid to overcome the problem with resonances at the North Pole. Also the error at the East Canadian coast and in the Norwegian Sea is higher than average. Here, the model has some difficulties to optimally simulate horizontal velocities. Overall, the error of modeled OBP gives a reasonable temporal and regional varying estimate and is a much better representation of the error than a globally uniform error assumption, which is constant over time.

3.2. Influence of modeled OBP error on the inverse solution

To investigate the influence of the modeled OBP error on the inverse solution, the inversion has been performed (1) with a constant error of 10 cm per $1.5^o \times 1.5^o$ grid cell and (2) using the modeled OBP error estimated in this study. For each week an error map is provided which shows in most regions a consistently smaller error than the previously assumed constant error. Only in some regions higher errors occur, such as in the Southern Ocean, west of the Drake passage. Introducing the varying error into the inversion increases the overall weighting of modeled OBP in the least squares estimation. The smaller the error of modeled OBP, the closer is the inverse solution to the model results.

Almost no differences in global mean ocean mass variations are introduced by the alternative error estimation of modeled OBP (Figure 2b). In GPS week 1202, the inverse solutions show a large offset in the ocean mean. This feature can be linked to the large amount of GRACE data gaps during that week combined with a different OBP error model. This means that OBP modeled with FESOM might strongly influence the inverse solutions, when the uncertainty of GRACE solutions is high.

The influence of the newly estimated error model on the mass correction term is small (Figure 2c). Including the mass correction term as part of the model forcing reduces the amplitude of the modeled global ocean mass variation to values similar to those from the inversion (Figure 2d). Once the model has been calibrated with the mass correction parameter, the difference with the inverse solution is small. The remaining discrepancy is most likely due to the band-limited nature of the inverse solution, which is not uniquely consistent with the spatial domain in which the ocean model acts. The seasonal phase of the FESOM mean ocean mass variations coincides well with GRACE and the inverse solution. Modeled OBP and the weekly GRACE solutions show realistic signal structures, when comparing them with the two inverse solutions (Figure 2e).

Adding the error of modeled OBP to the inversion results in inverse solutions (Figure 3a and 3b) having less temporal variations, mainly in the polar regions as depicted in Figure 3c and 3d. In both inverse solutions, higher variations occur in high latitude coastal regions and are most likely caused by leakage of land signals.

3.3. Validation with in-situ measurements

Measurements from OBPR at 100 locations distributed over the world ocean have been collected by several studies (*Kanzow et al.* [2005]; *Morison et al.* [2007]; *Park et al.* [2008], and others) and are assembled in a database [*Macrander et al.*, 2010]. We compared these measurements with the modeled weekly OBP anomalies, weekly GRACE measurements, and ocean mass variations from the two inverse solutions. We have computed the correlations and the RMS differences of the time series and OBPR data for different locations.

Modeled OBP and GRACE estimates generally show a good correlation with OBPR data but vary by region (Figure 4a and 4b). The correlation of modeled OBP is much higher (about 0.2) at the Kuroshio, at the South Drake Passage and in the Atlantic Ocean east of the Caribbean Sea (e.g. the array of the Meridional Overturning Variability Experiment (MOVE)) compared to GRACE estimates. Both estimates show high correlations with OBPR data in the Arctic Ocean and in the Southern Ocean, near the Kerguelen Islands, and low correlations at the Azores and the North Drake Passage. Correlations of GRACE with OBPR data are higher than FESOM with OBPR data at the Fram Strait and in the North Pacific, with a few exceptions. Note, that the applied Gauss filter influences the correlation between GRACE and OBPR data. Here, an averaging radius of 750 km [*Wahr et al.*, 1998] is chosen as it shows highest correlation for most timeseries.

The estimation of mass signals can be improved by combining different datasets, shown in Figure 4c. This is especially true for the MOVE array (Atlantic Ocean east of the Caribbean Sea), which is known to have low correlation compared with GRACE only solutions [*Kanzow et al.*, 2005]. Concerning the inverse results, a further increase of correlation is achieved when introducing the variable error of modeled OBP into the inversion as modeled OBP better represents the short term structures in OBPR measurements (Figure 4d). This particularly holds for the locations in the North Pacific (near Bering Sea), the cross section of the Antarctic Circumpolar Current (ACC) south of Africa, and the Kuroshio. Generally, the correlation of the inverse solutions with OBPR measurements strongly depends on the weighting of the individual datasets. If a dataset is highly correlated with OBPR data, but has a low weighting due to high uncertainties, the weighting becomes lower and some of the signals from this datasets may be damped in the inverse solution.

The influence of the weighting on the combinations of different data sets is also visible in Figure 5. Even with a constant error of modeled OBP, the inverse solution shows a higher correlation with OBPR measurements compared to the GRACE-only solutions at many positions. At some positions, however, the correlation decreases, e.g. the ACC crossing south of Africa. This is largely corrected when the estimated error of modeled OBP is applied. Compared to GRACE data, the correlation with OBPR data is increased by up to 0.5. Compared to the inversion with constant model error, the correlation with

OBPR data increased in all but three positions. Due to the high amount of deployments, the OBPR measurements at the Kuroshio Current are not included here, as they would distort the analysis.

Time series of the inverse solutions, modeled OBP, and weekly GRACE solutions (GSM+GAC) are compared with OBPR data at three example locations; one in the Southern Ocean and two in the North Atlantic (Figure 6 and 7a). Generally the short term signal structure is best represented by FESOM as most positions are more highly correlated with the OBPRs than for GRACE estimates. In contrast, the seasonal variations, which are not well modeled in the FESOM results, are captured in the GRACE solutions. The inverse solutions using the estimated variable error of modeled OBP has the best agreement with the temporal mass signal measured with OBPRs. The errors of GRACE and modeled OBP optimally trade off the advantages of both input data sets. Hence, this inverse solution represents both large scale variability and displays good correlations with OBPRs. This does not hold for the Arctic Ocean (see figure 7b). At this location, the mass signal of the inverse solution (including the variable error) is much less correlated to OBPRs than the signals of GRACE measurements and modeled OBP. Here, the inverse solution is not optimal, which indicates that there is still some potential for improvement, e.g. of the weighting scheme of the inversion.

In addition, we have calculated the RMS differences of our estimates minus the in-situ time series. The results confirm those found from the correlation analysis earlier. Figure 8a and 8b show the RMS between modeled OBP anomalies and GRACE estimates minus the measurements from the OBPRs. At many locations, modeled OBP shows a lower RMS difference with OBPRs than with GRACE estimates, for example in the equatorial

Atlantic Ocean where GRACE overestimates the variance of the signal. At these locations ocean mass variations are better estimated with the FESOM model. There are also many locations where the RMS differences of modeled OBP and GRACE estimates are similar, for example in the Southern Ocean south of Africa or at the Kerguelen Island. However, at some locations, such as in the Fram Strait or the Arctic Ocean, the RMS difference of the GRACE estimates indicate a better agreement in amplitude. At most locations, the residual RMS of the two inverse solutions show a better agreement in amplitude as compared to the GRACE estimates (Figure 8c and 8d). Only in the Arctic Ocean, the GRACE estimates show a lower residual RMS compared to the inverse estimates, and the inverse solutions also show poorer correlation.

The residual RMS of the inverse solution shows a slight improvement at almost all locations when the new OBP error model is used (Figure 9). Only one location south of Africa (AWI ANT3) shows higher residual RMS with the incorporation of the new OBP error model, as compared to when the constant error of modeled OBP is used. The poorer performance of the modeled OBP anomalies at this location is due to the strong variability caused by small scale eddies, which are not resolved by the coarse resolution of the model.

The differences between modeled OBP and OBPR measurements give an indication of the real error at these locations. A comparison of these errors to our perturbation-based error estimate reveals that they are of very similar magnitude (Figure 10). Generally the difference is located within the estimated error boundaries. At some positions the error is slightly overestimated, e.g. in the Mid Atlantic Ocean. Variability of the model error estimate is small. As expected, the difference sometimes exceeds the error estimate for a short time period, because of the stronger fluctuations of the short term signals in the OBPR measurements, but at least 84 % of the data remains within the estimated error boundaries (in mean 80 % of data remains at Kuroshio current).

4. Discussion and Conclusion

Weekly ocean mass variations, derived from the mass conserving FESOM model, show realistic geophysical patterns. However, no assimilation of altimetry data is performed within the FESOM model. Therefore, the error of modeled OBP derived by the FESOM model cannot be estimated on the basis of the error of the altimetry measurements as described by *Wu et al.* [2006]. It is known that the model results largely depend on the atmospheric conditions. For this reason, the error of modeled OBP is estimated by computing the differences between a second model simulation using an alternative atmospheric forcing field and the reference model simulation. The results include error maps which vary in time and space. Although the estimated error of modeled OBP does not include all possible error sources, it provides a realistic estimate with larger errors in regions where atmospheric conditions are uncertain, such as in the Southern Ocean west of the Drake Passage. In addition, in the Arctic Ocean and the Norwegian Sea the error is larger than average. In the open ocean the error of modeled OBP is about 4 cm, which is smaller than the more conservative assumed constant error of 10 cm as used in the first inversion. Overall the estimated error of modeled OBP displays geophysical patterns based on differences in atmospheric conditions, which makes it more realistic than an assumption of constant errors as used by *Rietbroek et al.* [2009]; *Wu et al.* [2006].

The joint estimation of mass redistribution of GRACE gravity data, GPS site displacements and modeled OBP highly depends on the weighting and therefore on the error estimation of the individual data sets [*Rietbroek et al.*, 2009]. By combining the different datasets, the estimation of ocean mass variations improved in many regions especially in the equatorial Atlantic Ocean where the correlation between OBPR data and GRACE measurements is quite low. In these locations, GRACE generally overestimates the variability of mass variations [*Kanzow et al.*, 2005]. Correlation and RMS difference are improved at many locations by introducing modeled OBP into the inversion as FESOM performs well on short term mass variations. GRACE is well suited to represent large-scale ocean mass variations on weekly time scales, which improves the representation of the seasonal variability of ocean mass in the inverse solutions. The inverse solution strongly depends on the weighting of the different input variables by their error estimates [*Wu et al.*, 2006; *Jansen et al.*, 2009a; *Rietbroek et al.*, 2009]. Introducing the estimated variable error of modeled OBP into the inversion further increases the correlation and lowers the RMS difference between ocean mass variations derived by the inversion and measurements from OBPR. Therefore, using the time- and space dependent error in a joint inversion of independent data sets improves the estimation of ocean mass changes.

The mass budget of the FESOM model directly depends on the forcing parameters: precipitation, evaporation, and river runoff. These forcing data generally arise from models which do not conserve mass, and which are therefore not consistent with each other. Consequently, their errors, arising from both the assimilated data and the model itself, propagate as large uncertainties in the ocean models [*Kalnay*, 1996; *Hagemann et al.*, 2005; *Berrisford*, 2009]. This results in an unrealistic long term trend and high uncertainties in the mass budget of the model, which should be treated with caution. However, the comparison between other studies [*Chambers, et al.*, 2004; *Wu et al.*, 2006; *Wenzel* *and Schröter*, 1998; *Willis et al.*, 2008], the inverse solutions, and the model results show that simulated weekly global mean ocean mass variations have similar phase, only the modeled amplitude is slightly overestimated. This can be improved by introducing the mass correction term from the inversion into the model, as a scaling to precipitation. This correction adjusts the modeled mass budget to the one of the inverse solution, and therefore gives the possibility not only to analyze modeled ocean mass variation, but also to investigate long term trends as soon as longer time series are available.

Acknowledgments. The authors acknowledge support provided by the German Research Foundation (DFG) under grants KU 1207/6-1, FL 592/1-1, and SCHR779/4-1 within the Special Priority Program SPP 1257 Mass Transport and Mass Distribution in the System Earth. The Arctic BPR data were kindly provided by James Morison, whose research were funded under National Science Foundation Grant OPP 0326109:"Ocean Pressure in the Arctic Derived from Satellite Gravity and In Situ Pressure Measurements". Furthermore, we would like to thank the ECMWF data center for providing atmospheric datasets from ERA-Interim and the ERA40 reanalyzes as well as for the operational ECMWF analysis data. We would like to thank the NOAA Climate Diagnostics Center, Boulder for providing the NCEP/NCAR reanalyzes online at http://www.cdc.noaa.gov. In addition, we would like to thank Christoph Dahle for providing weekly GRACE solutions used in the inversion and Robert Dill for providing river runoff from the LSDM model. Finally, we thank the anonymous reviewers for their helpful comments.

References

Blewitt, G. (2003), Self-consistency in reference frames, geocenter definition, and surface loading of the solid Earth, *Journal of Geophysical Research, 108 (B2), 2103*, doi: 10.1029/2002JB002082.

Berrisford, P., D. Dee, K. Fielding, M. Fuentes, P. Kallberg, S. Kobayashi, and S. Uppala (2009). The era-interim archive. ERA Report Series, ECMWF.

Bingham, R. J. and C. W. Hughes (2006), Observing seasonal bottom pressure variability in the North Pacific with GRACE, *Geophysical Research Letters, 33*, L08607, doi: 10.1029/2005GL025489.

Böning, C., R. Timmermann, A. Macrander, and J. Schröter (2008), A pattern-filtering method for the determination of ocean bottom pressure anomalies from GRACE solutions, *Geophysical Research Letters, 35*, doi:10.1029/2008GL034974.

Böning, C. (2009), Validation of ocean mass variability derived from the Gravity Recovery and Climate Experiment - Studies utilizing in-situ observations and results from a Finite Element Sea-ice Ocean Model, Dissertation, *University of Bremen, Bremen, Germany.*

Chen, J., C. Wilson, K.-W. Seo (2009), S2 tide aliasing in GRACE time-variable gravity solutions, *Journal of Geodesy, Springer Berlin, Heidelberg, Germany, issn: 0949-7714, 83,7,679-687*, doi: 10.1007/s00190-008-0282-1.

Chambers, D. P., J. Wahr, and R. S. Nerem (2004), Preliminary observations of global ocean mass variations with GRACE, *Geophysical Research Letters,31*, L13310, doi:10.1029/2004GL020461.

Chambers, D. P. (2006), Evaluation of the new GRACE time-variable gravity data over the ocean, *Geophysical Research Letters, 33*, L17603, doi: 10.1029/2006GL27296.

Chambers, D. P. and J. K. Willis (2009), Low-frequency exchange of mass between ocean basins, *Journal of Geophysical Research, 114*, C11008, doi: 10.1029/2009JC005518.

Dahle, Ch., F. Flechtner, J. Kusche, and R. Rietbroek (2008), *GFZ EIGEN-GRACE05S (RL04) Weekly Gravity Field Time Series, Proceedings of the 2008 GRACE Science Team Meeting, San Francisco, December 12./13.2008*, http://www.csr.utexas.edu/grace/GSTM.

Danilov, S. and N. Yakovlev (2003), A Finite Element Ice Model.

Danilov, S., G. Kivman and J. Schröter (2004), A finite-element ocean model: principles and evaluation, *Ocean Modelling,6,2,125-150*, doi:10.1016/S1463-5003(02)00063-X.

Danilov, S., G. Kivman and J. Schröter (2005), Evaluation of an eddy-permitting finite-element ocean model in the North Atlantic, *Ocean Modelling, 10, 35-49*, doi: 10.1016/j.ocemod.2004.07.006.

Dill, R. (2008), Hydrological model LSDM for operational earth rotation and gravity field variations, *Scientific Technical Report; 08/09, Helmholtz-Zentrum Potsdam Deutsches GeoForschungsZentrum, 37*, doi: 10.2312/GFZ.b103-08095.

Dobslaw, H. and M. Thomas, Simulation and observation of global ocean mass anomalies, *Journal of Geophysical Research, 112*, C05040, doi: 10.1029/2006JC004035.

Flechtner, F., C. Dahle, K. H. Neumayer, R. König, and C. Förste (2010), The release 04 champ and grace eigen gravity field models, *System Earth via Geodetic-Geophysical Space Techniques, Adv. Technologies in Earth Sciences , 41.*

ECMWF (1995). The Description of the ECMWF/WCRP Level III-A *Global Atmospheric Data Archive.*

Greatbatch, R. J. (1994), A note on the representation of steric sea level in models 812 that conserve volume rather than mass, *Journal of Geophysical Research, 99, 12,767-12,771*, doi:10.1029/94JC00847.

Hagemann, S., K. Arpe, and L. Bengtsson (2005), Validation of the hydrological cycle of era-40. ERA-40 Project Report Series, *ECMWF*, http://www.ecmwf.int/publications/library/do/references/list/192.

Jansen, M. J. F., B. C. Gunter, and J. Kusche (2009), The impact of GRACE, GPS, and OBP data on estimates of global mass redistribution, *Geophys. J. Int. 177, 1-13*, doi: 10.1111/j.1365-246X.2008.04031.x.

Jansen, M. J. F., B. C. Gunter, R. Rietbroek, C. Dahle, J. Kusche, F. Flechnter, S-E. Brunnabend, and J. Schröter (2009), Estimating sub-monthly global mass transport signals using GRACE, GPS, OBP data sets, *In: Proc. of the IAG International Symposium on Gravity, Geoid and Earth Observation (GGEO2008), Chania, Crete, June 23-27, 2008.*

Kalnay E., M. Kanamitsu, R. Kistler, W. Collins, D. Deaven, L. Gandin, M. Iredell, S. Saha, G. White, J. Woollen, Y. Zhu, M. Chelliah, W. Ebisuzaki, W. Higgins, J. Janowiak, K.C. Mo, C. Ropelewski, J. Wang, A. Leetmaa, R. Reynolds, Roy Jenne, and D. Joseph (1996), The NCEP/NCAR 40-year reanalyses project, *Bull. Amer. Met. Soc., 77, 437-471.*

Kanzow, T., F. Flechtner, A. Chave, R. Schmidt, P. Schwintzer, and U. Send (2005), Seasonal variation of ocean bottom pressure derived from Gravity Recovery and Climate Experiment (GRACE): Local validation and global patterns, *Journal of Geophysical Research, 110*, C09001, doi:10.1029/2004JC002772.

Kusche, J. and E. J. O. Schrama (2005), Surface mass redistribution inversion from global GPS deformation and Gravity Recovery and Climate Experiment (GRACE) gravity data, *Journal of Geophysical Research (Solid Earth), 110(B9)*, 9409ff., doi:10.1029/2004/JB003556.

Kusche, J. (2007), Approximate decorrelation and non-isotropic smoothing of time-variable GRACE-type gravity field models, *Journal of Geodesy, 81 (11), 733-749*, doi:10.1007/s00190-007-0143-3.

Macrander, A., C. Böning, O. Boebel, and J. Schröter (2010), Validation of GRACE Gravity Fields by in-situ Data of Ocean Bottom Pressure, in *Stroink, L., V. Mosbrugger, G. Wefer, F. M. Flechtner, Th. Gruber, A. Güntner, M. Mandea, M. Rothacher, T. Schöne and J. Wickert, System Earth via Geodetic-Geophysical Space Techniques, Advanced Technologies in Earth Sciences, 169-185, Springer Berlin Heidelberg, Germany, isbn: 978-3-642-10228-8*, doi: 10.1007/978-3-642-10228-8-14.

Morison, J., J. Wahr, R. Kwok, and C. Peralta-Ferriz (2007), Recent trends in Arctic Ocean mass distribution revealed by GRACE, *Geophysical Research Letters, 34*, doi:10.1029/2006GL029016.

Park, J.-H., D. R. Watts, K. A. Donohue, and S. R. Jayne (2008), A comparison of in situ bottom pressure array measurements with GRACE estimates in the Kuroshio Extension, *Geophysical Research Letters, 35*, L17601, doi:10.1029/2008GL034778

Ponte, R. M., K. J. Quinn, C. Wunsch, and P. Heimbach (2007), A comparison of model and GRACE estimates of large-scale seasonal cycle in ocean bottom pressure, *Geophysical Research Letters, 34*, L09603, doi: 10.1029/2007GL029599.

Quinn, K. J. and R. M. Ponte (2010), Uncertainty in ocean mass trends from GRACE, *Geophysical Journal International, 181, 762-768*, doi:10.1111/j.1365-246X.2010.04508.x.

Rietbroek, R., P. LeGrand, B. Wouters, J.-M. Lemoine, G. Ramillien, and C. W. Hughes (2006), Comparison of in situ bottom pressure data with GRACE gravimetry in the Crozet-Kerguelen region, *Geophys. Res. Lett., 33*, L21601, doi: 10.1029/2006GL027452.

Rietbroek R., S.-E. Brunnabend, Ch. Dahle, J. Kusche, F. Flechtner, J. Schröter, and R. Timmermann (2009), Changes in total ocean mass derived from GRACE, GPS, and Ocean Modelling with weekly Resolution, *Journal of Geophysical Research (Oceans), 144*, C11004, doi: 10.1029/2009JC005449.

Seo, K.-W., C. R. Wilson, J. Chen, D. E. Wilson (2008), GRACE's spatial aliasing error, *Geophys. J. Int. 172, 41-48* doi: 10.1111/j.1365-246X.2007.03611.x.

Swenson, S. C. and J. Wahr (2006), Post-processing removal of correlated errors in GRACE data, *Geophysical Research Letters, 33*, L08402, doi: 10.1029/2005GL025285.

Swenson, S, C. Chambers, and J. Wahr (2008), Estimating geocenter variations from a combination of GRACE and ocean model output, *Journal of Geophysical Research, 113*, B08410, doi: 10.1029/2007JB005338.

Simmons, A., S. Uppala, D. Dee, and S. Kobayashi (2006), Era-interim: New ecmwf reanalysis products from 1989 onwards, *ECMWF Newsletter, 110*, http://www.ecmwf.int/publications/newsletters/pdf/.

Stammer, D., C. Wunsch, I. Fukumori, and J. Marshall (2002), State estimation in modern oceanographic research, *EOS, Transactions, American Geophysical Union, 83, 27, 294-295, 289*.

Tabley, B., S. Bettadpur, M. Watkins, and C. Reigber (2004), The gravity recovery and climate experiment: Mission overview and early gravity results, *Geophysical Research Letters, 31*, L09607, doi: 10.1029/2003GL019920.

Timmermann, R., S. Danilov, J. Schröter, C. Böning, D. Sidorenko, and K. Rollenhagen (2009), Ocean circulation and sea ice distribution in a finite element global sea ice – ocean model, *Ocean Modelling, 27, 114-129*, doi:10.1016/j.ocemod.2008.10.009.

Thomson, P., S. Bettadpur, and B. Tapley (2004), Impact of short term period, non-tidal, temporal mass variability on GRACE estimates, *Geophysical Research Letters, 31*, L006619, doi: 10.1029/2003GL019285.

Uppala, S.M., P.W. Kallberg, A. J. Simmons, U. Andrae, V. da Costa Bechtold, M. Fiorino, J. K. Gibson, J. Haseler, A. Hernandez, G. A. Kelly, X. Li, K. Onogi, S. Saarinen, N. Sokka, R. P. Allan, E. Andersson, K. Arpe, M. A. Balmaseda, A. C. M. Beljaars, L. van de Berg, J. Bidlot, N. Bormann, S. Caires, F. Chevallier, A. Dethof, M. Dragosavac, M. Fisher, M. Fuentes, S. Hagemann, E. Holm, B. J. Hoskins, L. Lsaksen, P. A. E. M. Janssen, R. Jenne, A. P. McNally, J.-F. Mahfouf, J.-J. Morcrette, N. A. Rayner, R. W. Saunders, P. Simon, A. Sterl, K. E. Trenberth, A. Untch, D. Vasiljevic, P. Viterbo, and J. Woollen (2005), The ERA-40 re-analysis, *Quart. J. R. Meteorol. Soc., 131, 2961-3012*, doi: 10.1256/qj.04.176.

Wahr, J., M. Molenaar, and F. Bryan (1998), Time variable of the Earth's gravity field: Hydrological and oceanic effects and their possible detection using GRACE, *Journal of Geophysical Research, 103*, B12, pp.30205-30229, doi:10.1029/98JB02844.

Wenzel, M., and J. Schröter (2007), The global ocean mass budget in 1993 - 2003 estimated from sea level change, *Journal Physical Oceanography, 37, 203-213*, doi:10.1175/JPO3007.1.

Willis, J. K., D. P. Chambers, and R. S. Nerem (2008), Assessing the globally averaged sea level budget on seasonal to interannual timescales, *Journal of Geophysical Research, 113*, C06015, doi:10.1029/2007JC004517.

Wu, X., M. B. Heflin, E. R. Ivins, and I. Fukumori (2006), Seasonal and interannual global surface mass variations from multi-satellite geodetic data, *Journal of Geophysical Research, 111*, B09401, doi:10.1029/2005JB004100.

Wu, X., M. B. Heflin, H. Schotman, B. L. A. Vermeersen, D. Dong, R. S. Gross, E. R. Ivins, A. W. Moore, and S. E. Owen (2010), Simultaneous estimation of global present-day water transport and glacial isostatic adjustment, *Nature Geoscience, 3, 642-646*, doi:10.1038/ngeo938.

Figure 1. Modeled OBP anomalies and its error in meter equivalent water height (a): OBP anomalies of week 1400 (05^{th}-11^{th} November 2006) using NCAR/NCEP forcing, (b): Standard deviation of weekly mean OBP anomalies using NCAR/NCEP forcing (time range: 2003-2007), (c): Modeled OBP error of week 1400, (d): Variations of local mean error of modeled OBP (time range: 2003-2007), (e): Error of GRACE estimate of week 1400, and (f): Standard deviation of weekly mass anomalies estimated from GRACE where a 750 km Gauss filter is applied (time range: 2003-2007); note that off-scale values are colored black

Figure 2. Weekly global mean ocean mass anomalies in equivalent water height (a): Modeled OBP forced by different atmospheric datasets (b): Inverse solutions (c): Mass correction terms (d): OBP modeled with improved fresh water cycle (mass correction term applied) (e): Comparison with GRACE (GSM+GAC, 750 km Gauss filter applied)

Figure 3. Inverse solutions in meter equivalent water height (a): Inverse solution using constant error of modeled OBP of week 1400 (05^{th}-11^{th} November 2006), (b): Inverse solution using variable error of modeled OBP week 1400 (05^{th}-11^{th} November 2006), (c): Standard deviation of inverse solution for weeks 1204 to 1459 using constant error of modeled OBP, and (d): Standard deviation of inverse solution for weeks 1204 to 1459 using variable error of modeled OBP

Figure 4. Correlation with in-situ bottom pressure (OBPR) for (a): Modeled OBP (FESOM forced with atmospheric data from NCAR/NCEP), (b): GRACE solution GSMGAC (750 km Gauss filter applied), (c): The inverse solution using constant error of modeled OBP, and (d): The inverse solution using variable error of modeled OBP; if the correlation is significant at a location (on a 95% significant level), the position is marked with a bold black circle.

Figure 5. Histogram of the differences between correlations with OBPR measurements and (a): Inversion (constant OBP error applied) and weekly GRACE (750 km Gauss filter applied), (b): Inversion (variable OBP error applied) and weekly GRACE (750 km Gauss filter applied), as well as (c): Inversion (variable OBP error applied) and Inversion (constant OBP error applied)

Figure 6. Comparison of ocean bottom pressure timeseries with OBPR data at location (a): MOVE M3 (Atlantic Ocean, east of the Caribbean Sea) (b): POL SD2 (South East of the Drake Passage)

Figure 7. Comparison of ocean bottom pressure timeseries with OBPR data at location (a): RAPID MAR3 (Mid Atlantic Ocean) and (b): mean of station ABPR1 and ABPR3 (Arctic Ocean)

Figure 8. Root mean Square of differences of in-situ bottom pressure measurements and (a): GRACE (GSM+GAC, 750 km Gauss filter applied), (b): Modelled OBP, (c): The inverse solution using constant error of modeled OBP, and (d): The inverse solution using variable error of modeled OBP

Figure 9. Histogram of the root mean square differences between correlations with OBPR measurements and (a): Inversion (constant OBP error applied) and weekly GRACE (750 km Gauss filter applied), (b): Inversion (variable OBP error applied) and weekly GRACE (750 km Gauss filter applied), as well as (c): Inversion (variable OBP error applied) and Inversion (constant OBP error applied)

Figure 10. Comparison of modeled OBP error (red) with the difference of modeled OBP and OBPR measurements (blue) for locations (a): KESS E7 (Kuroshio), (b): AWI F8 (Framstrait), MOVE M3 (Atlantic Ocean, east of the Caribbean Sea) , and CNES AMS (near New Amsterdam, about 10^o north-east of the Kerguelen Islands)

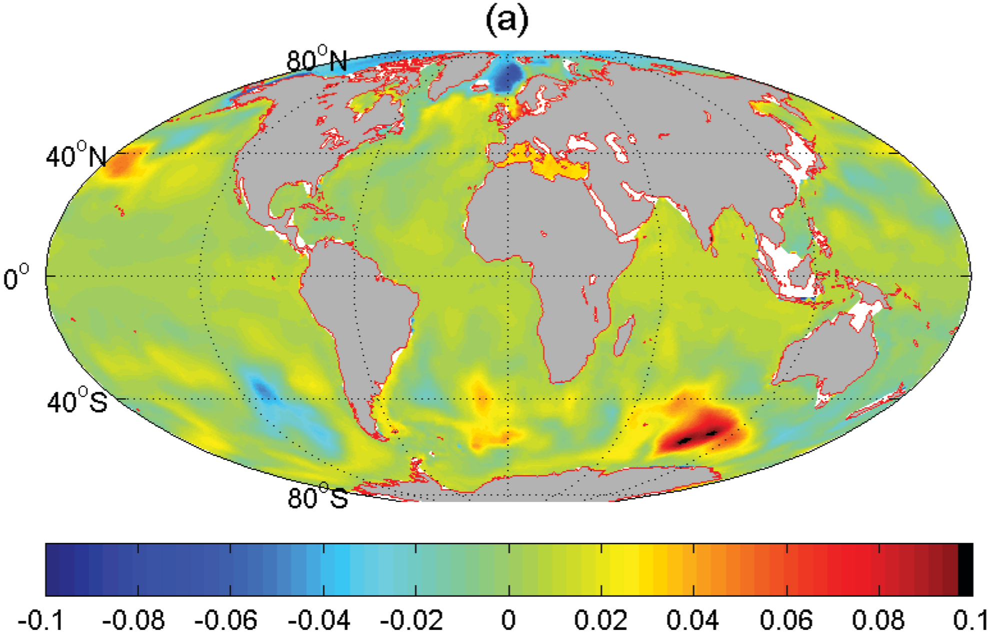
(a)
80°N
40°N
0°
40°S
80°S
-0.1
-0.08
-0.06
-0.04
-0.02
0
0.02
0.04
0.06
0.08
0.1

(b)

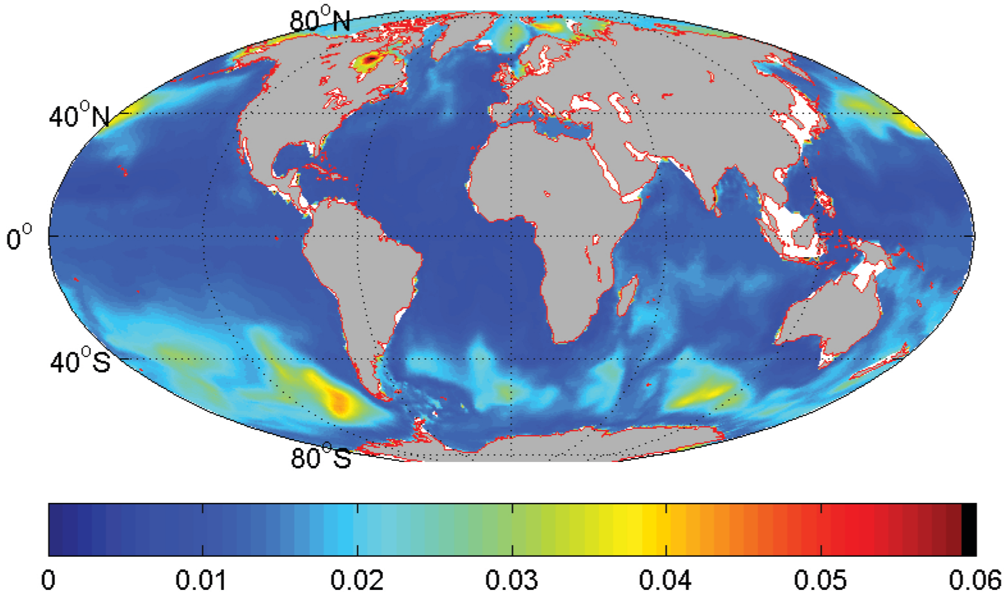

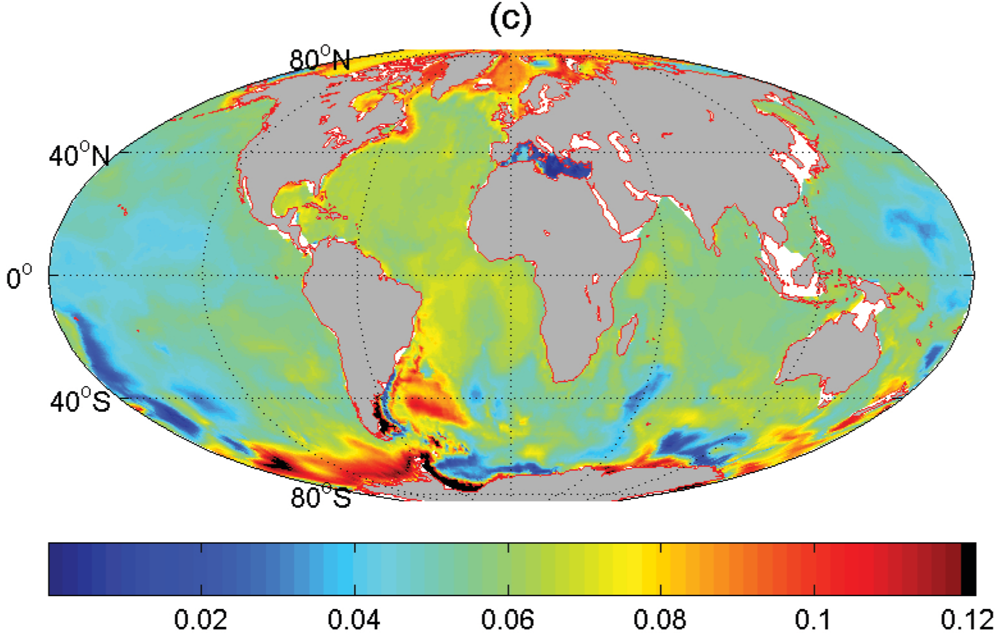

(c)
80°N
40°N
0°
40°S
80°S
0.02
0.04
0.06
0.08
0.1
0.12

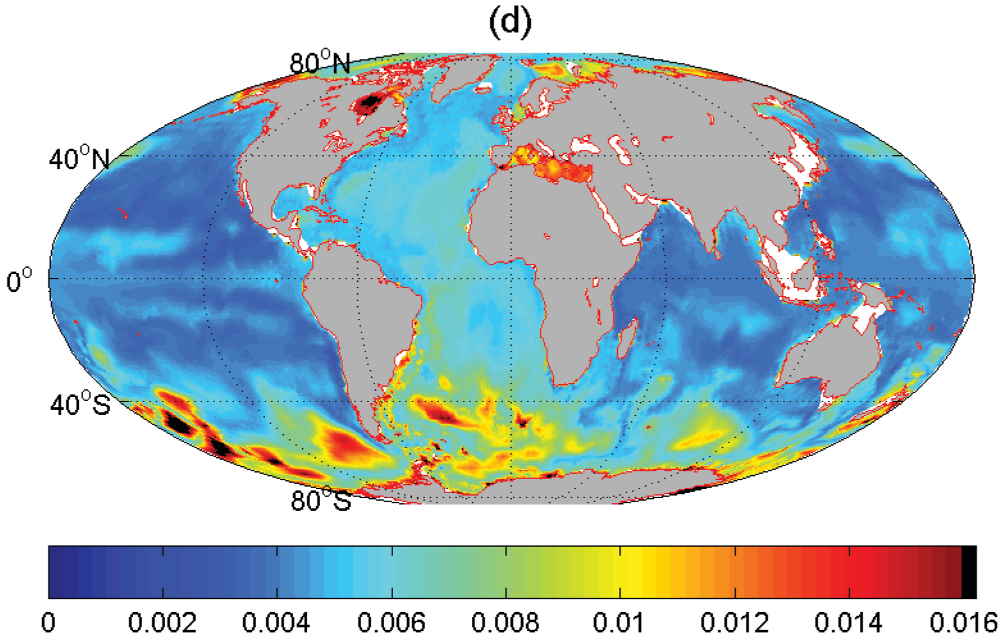
(d)
80°N
40°N
0°
40°S
80°S
0
0.002
0.004
0.006
0.008
0.01
0.012
0.014
0.016

(e)

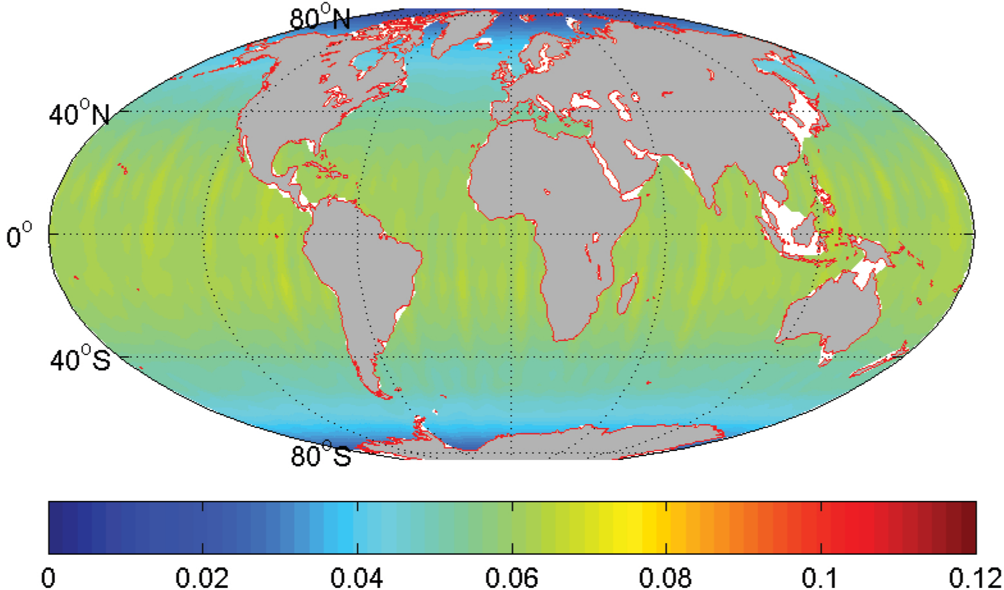

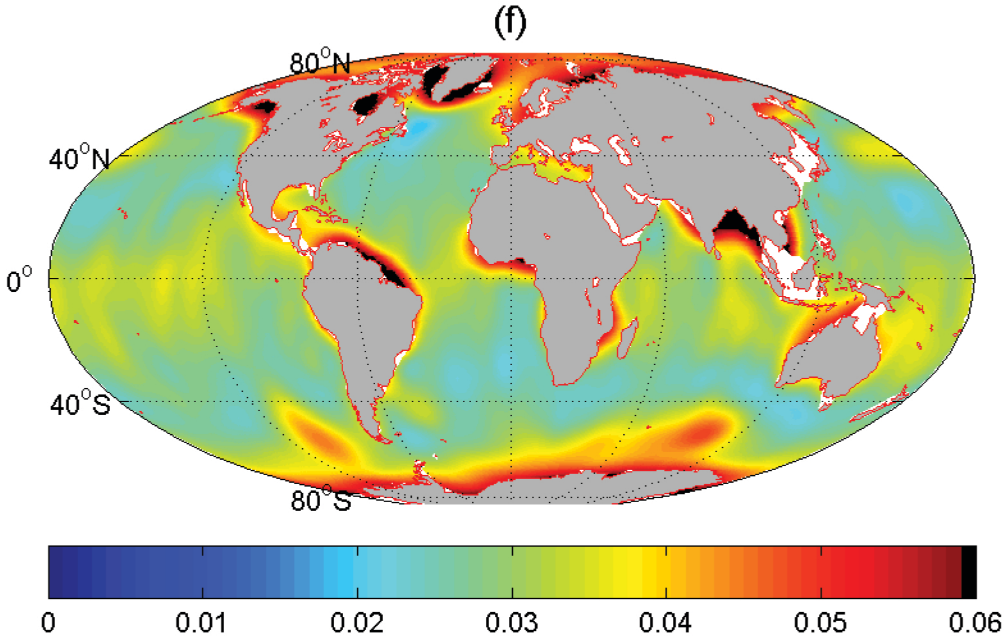
(f)
80°N
40°N
0°
40°S
80°S
0
0.01
0.02
0.03
0.04
0.05
0.06

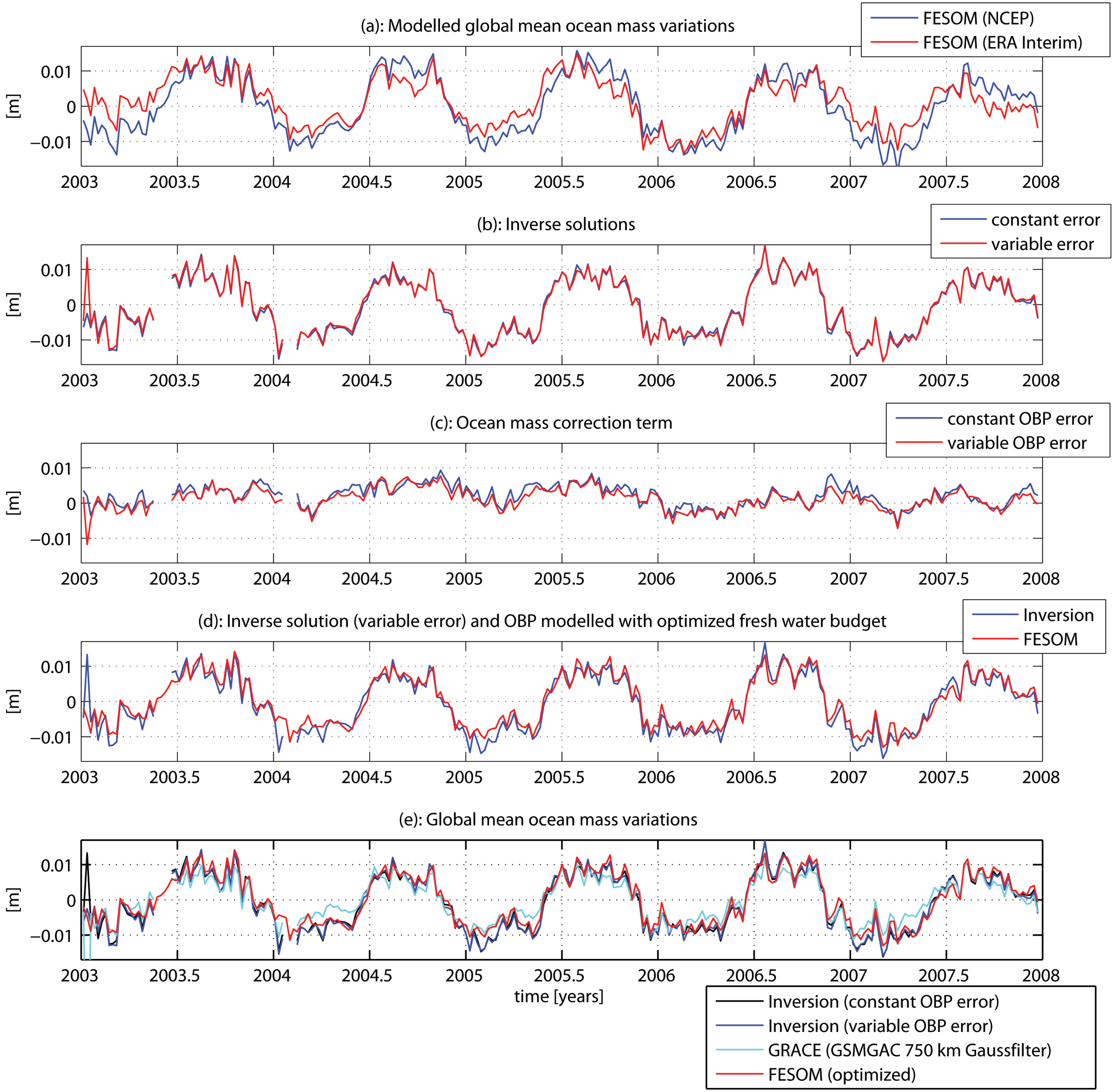

(a): Modelled global mean ocean mass variations
FESOM (NCEP)
FESOM (ERA Interim)
(b): Inverse solutions
constant error
variable error
(c): Ocean mass correction term
constant OBP error
variable OBP error
(d): Inverse solution (variable error) and OBP modelled with optimized fresh water budget
Inversion
FESOM
(e): Global mean ocean mass variations
[m]
0.01
0
−0.01
2003
2003.5
2004
2004.5
2005
2005.5
2006
2006.5
2007
2007.5
2008
time [years]
Inversion (constant OBP error)
Inversion (variable OBP error)
GRACE (GSMGAC 750 km Gaussfilter)
FESOM (optimized)

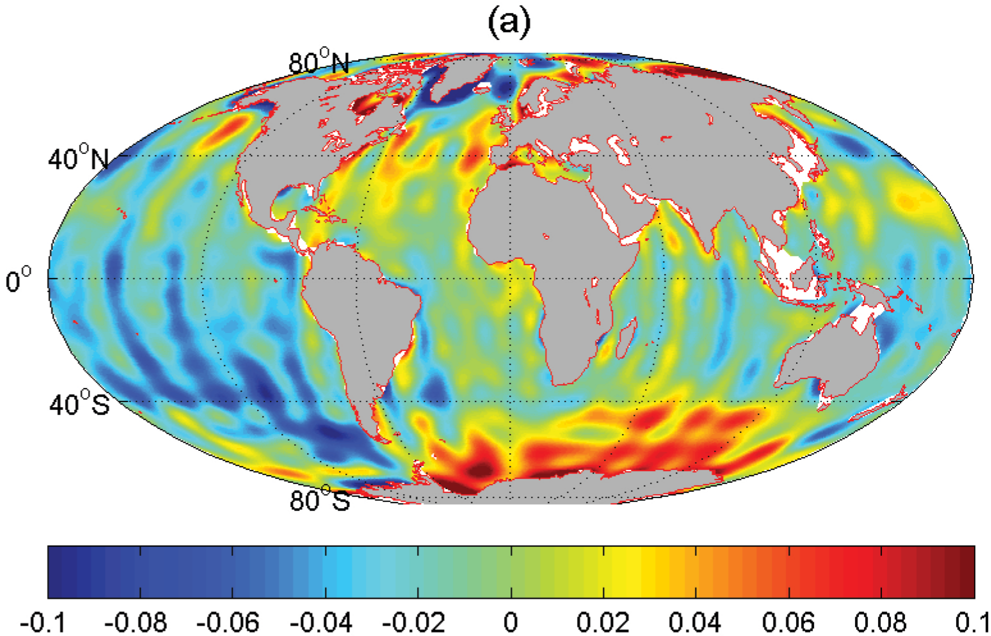

(a)
80°N
40°N
0°
40°S
80°S
-0.1
-0.08
-0.06
-0.04
-0.02
0
0.02
0.04
0.06
0.08
0.1

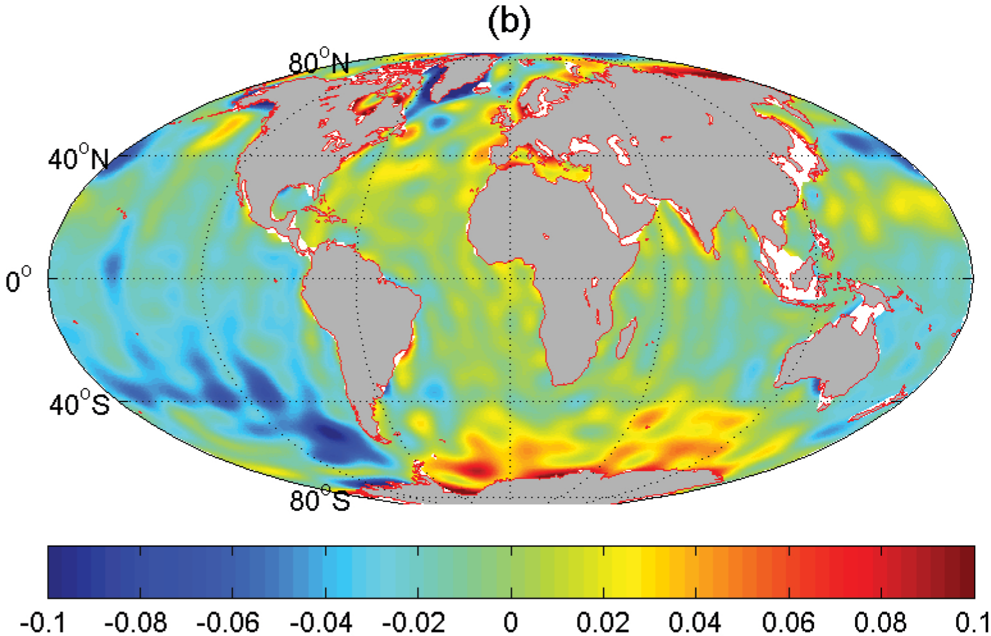
(b)
80°N
40°N
0°
40°S
80°S
-0.1
-0.08
-0.06
-0.04
-0.02
0
0.02
0.04
0.06
0.08
0.1

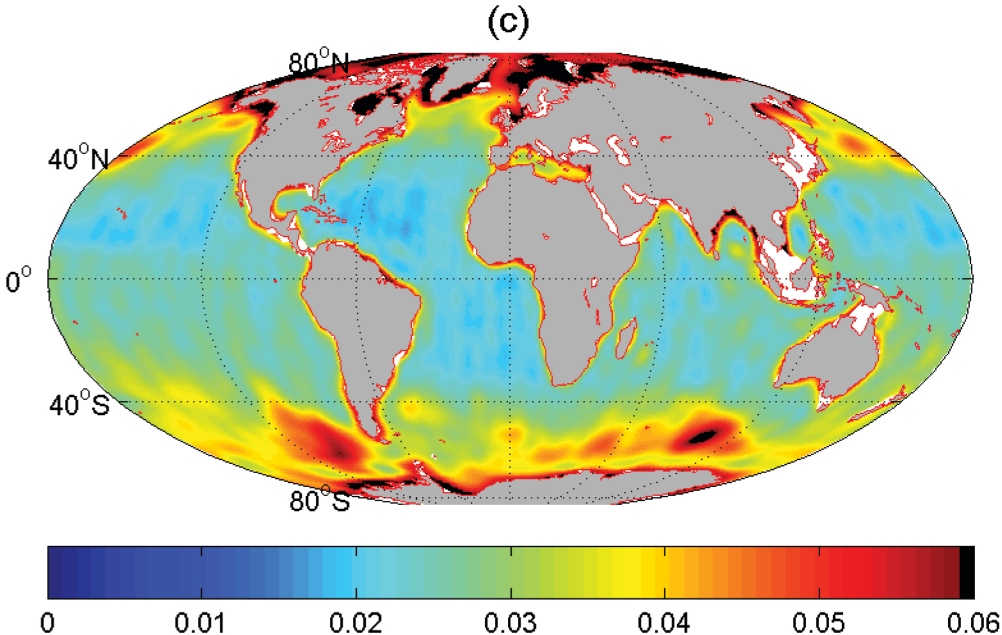
(c)
80°N
40°N
0°
40°S
80°S
0
0.01
0.02
0.03
0.04
0.05
0.06

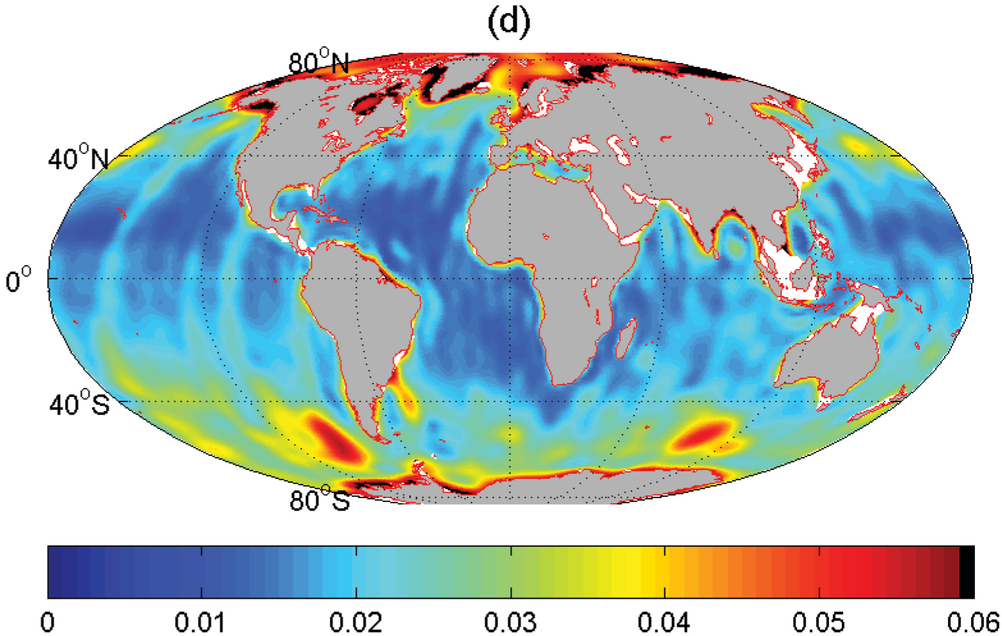
(d)
80°N
40°N
0°
40°S
80°S
0
0.01
0.02
0.03
0.04
0.05
0.06

(a)

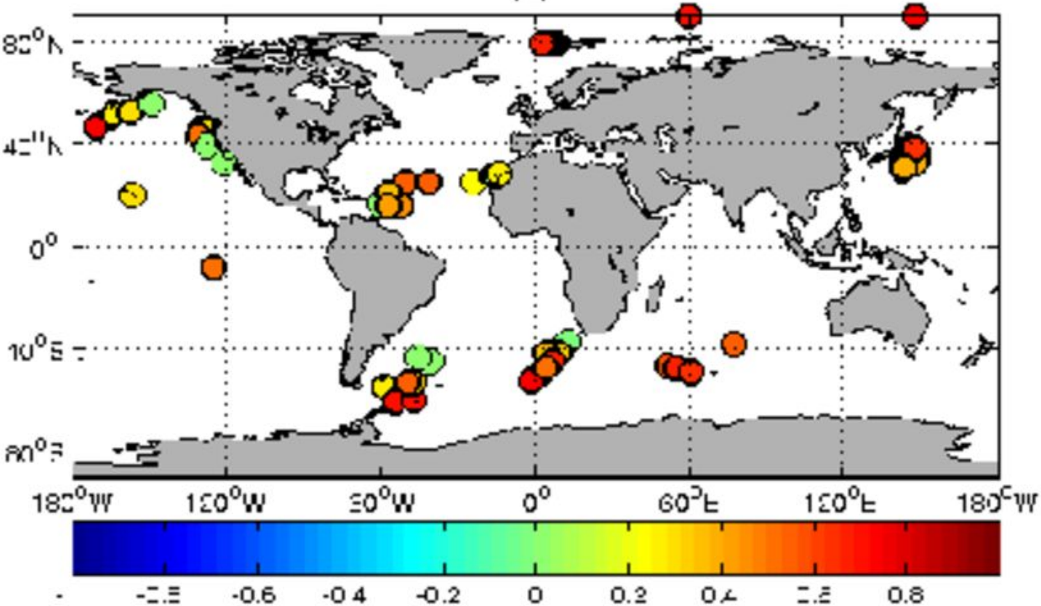

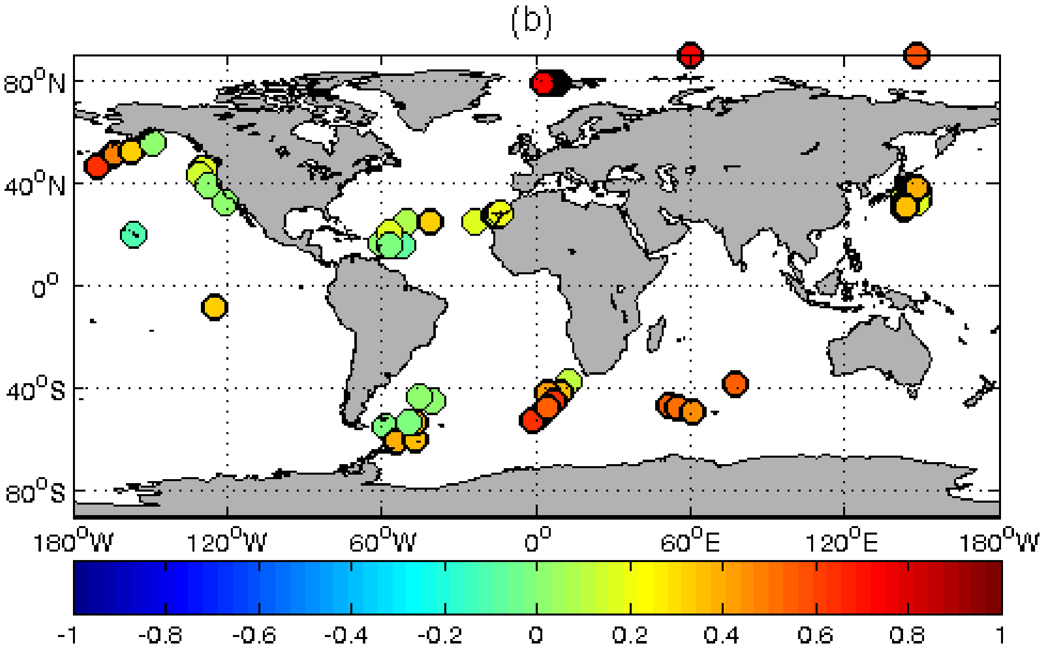
(b)
80⁰N
40⁰N
0⁰
40⁰S
80⁰S
180⁰W
120⁰W
60⁰W
0⁰
60⁰E
120⁰E
180⁰W
-1
-0.8
-0.6
-0.4
-0.2
0
0.2
0.4
0.6
0.8
1

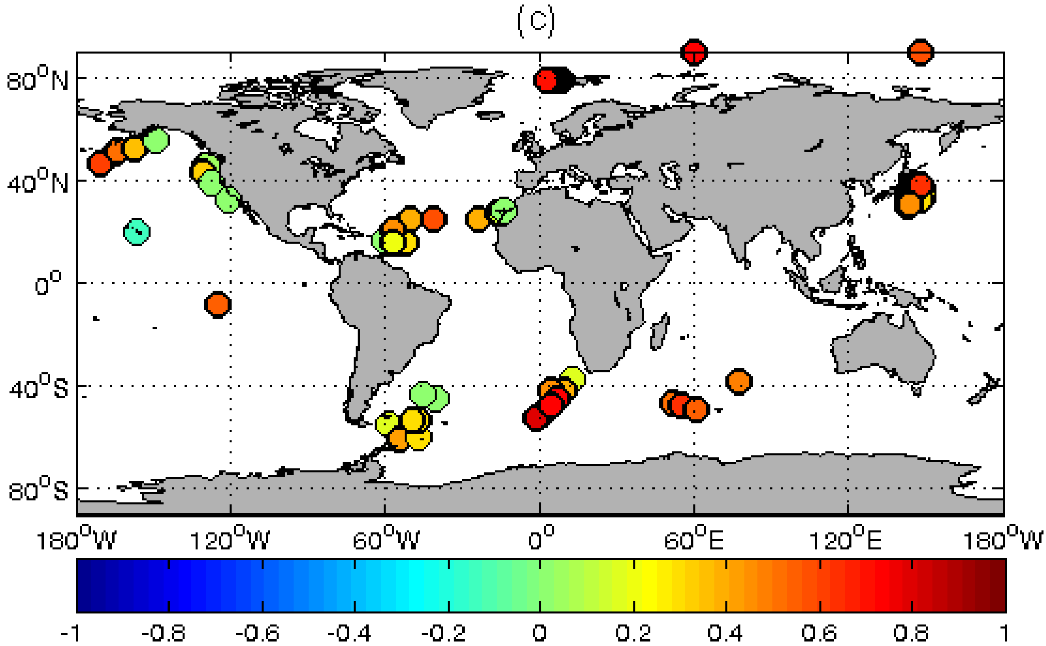
(c)
80°N
40°N
0°
40°S
80°S
180°W
120°W
60°W
0°
60°E
120°E
180°W
-1
-0.8
-0.6
-0.4
-0.2
0
0.2
0.4
0.6
0.8
1

(d)

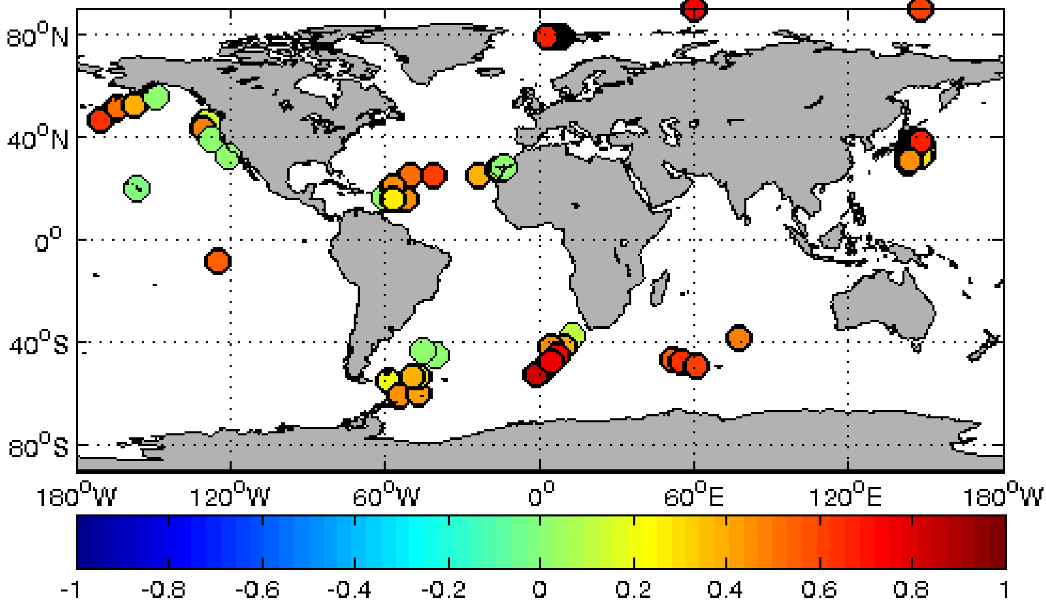

80°N
40°N
0°
40°S
80°S
180°W
120°W
60°W
0°
60°E
120°E
180°W
-1
-0.8
-0.6
-0.4
-0.2
0
0.2
0.4
0.6
0.8
1

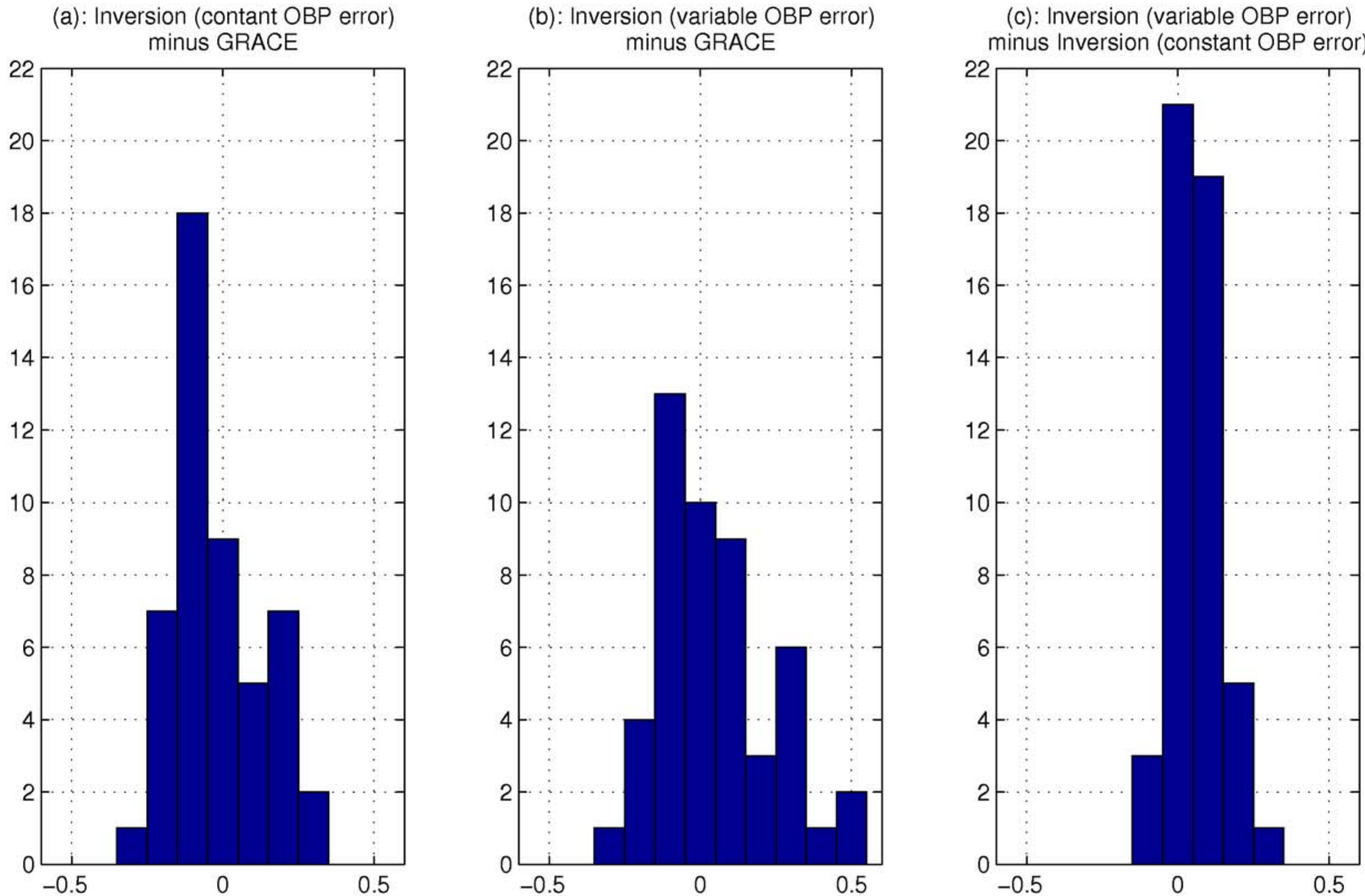
(a): Inversion (contant OBP error)
minus GRACE
(b): Inversion (variable OBP error)
minus GRACE
(c): Inversion (variable OBP error)
minus Inversion (constant OBP error)
0
2
4
6
8
10
12
14
16
18
20
22
−0.5
0
0.5

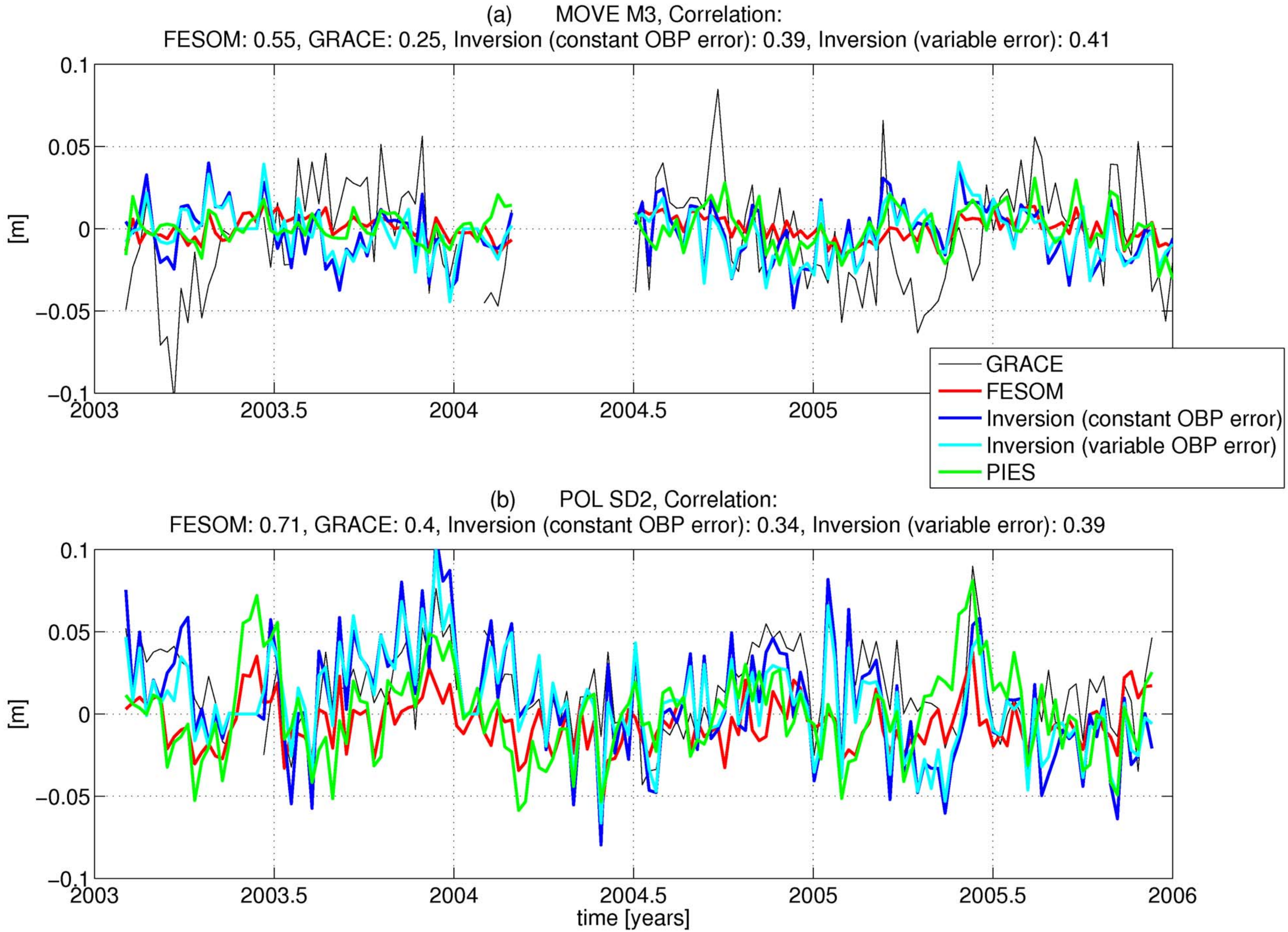
(a) MOVE M3, Correlation:
FESOM: 0.55, GRACE: 0.25, Inversion (constant OBP error): 0.39, Inversion (variable error): 0.41
[m]
0.1
0.05
0
−0.05
−0.1
2003
2003.5
2004
2004.5
2005
GRACE
FESOM
Inversion (constant OBP error)
Inversion (variable OBP error)
PIES
(b) POL SD2, Correlation:
FESOM: 0.71, GRACE: 0.4, Inversion (constant OBP error): 0.34, Inversion (variable error): 0.39
[m]
0.1
0.05
0
−0.05
−0.1
2003
2003.5
2004
2004.5
2005
2005.5
2006
time [years]

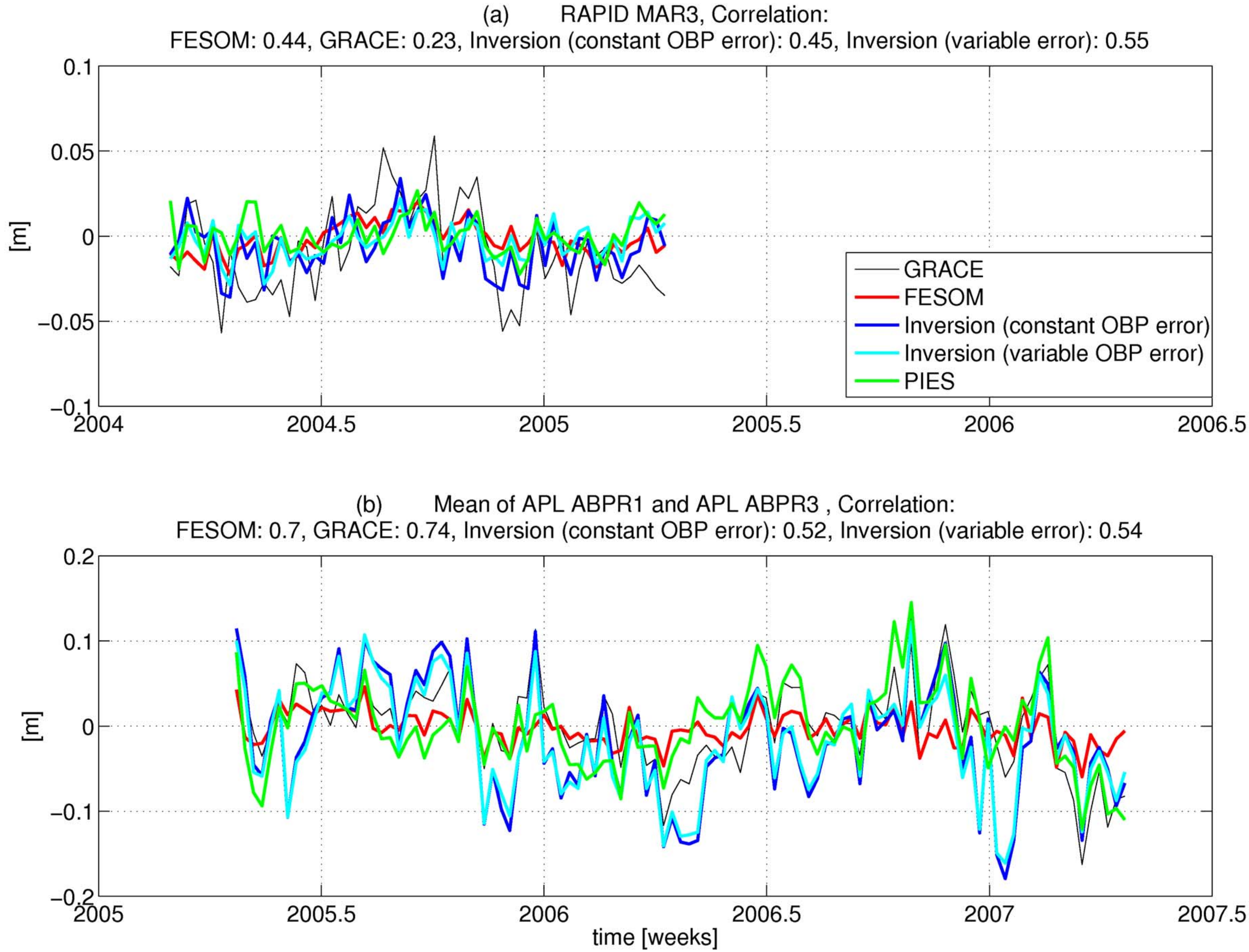
(a) RAPID MAR3, Correlation:
FESOM: 0.44, GRACE: 0.23, Inversion (constant OBP error): 0.45, Inversion (variable error): 0.55
0.1
0.05
0
−0.05
−0.1
[m]
2004
2004.5
2005
2005.5
2006
2006.5
GRACE
FESOM
Inversion (constant OBP error)
Inversion (variable OBP error)
PIES
(b) Mean of APL ABPR1 and APL ABPR3 , Correlation:
FESOM: 0.7, GRACE: 0.74, Inversion (constant OBP error): 0.52, Inversion (variable error): 0.54
0.2
0.1
0
−0.1
−0.2
[m]
2005
2005.5
2006
2006.5
2007
2007.5
time [weeks]

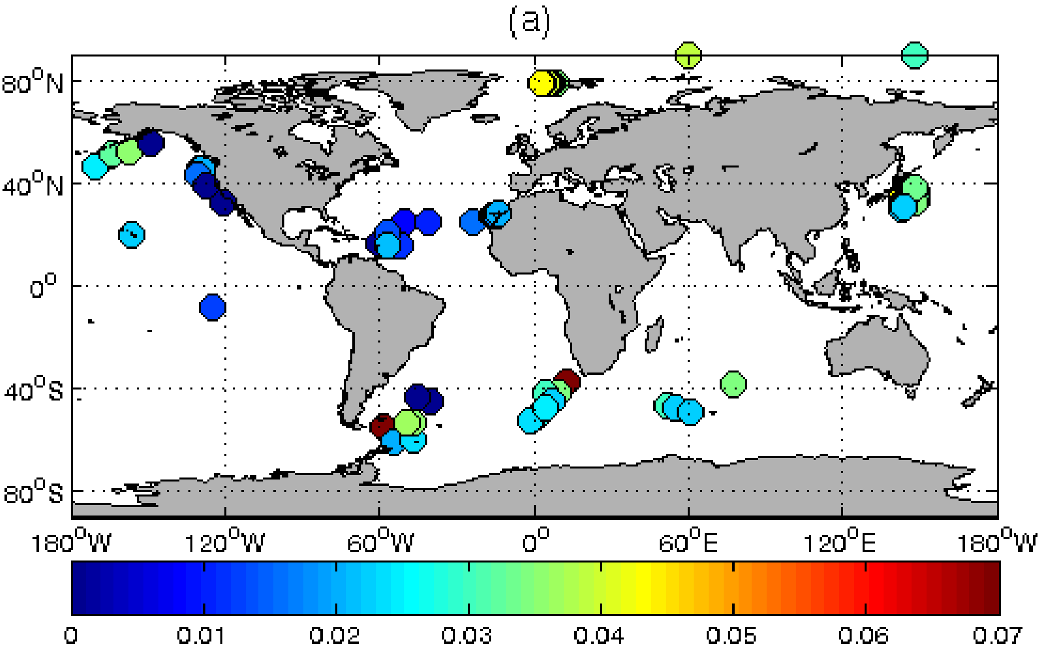
(a)
80°N
40°N
0°
40°S
80°S
180°W
120°W
60°W
0°
60°E
120°E
180°W
0
0.01
0.02
0.03
0.04
0.05
0.06
0.07

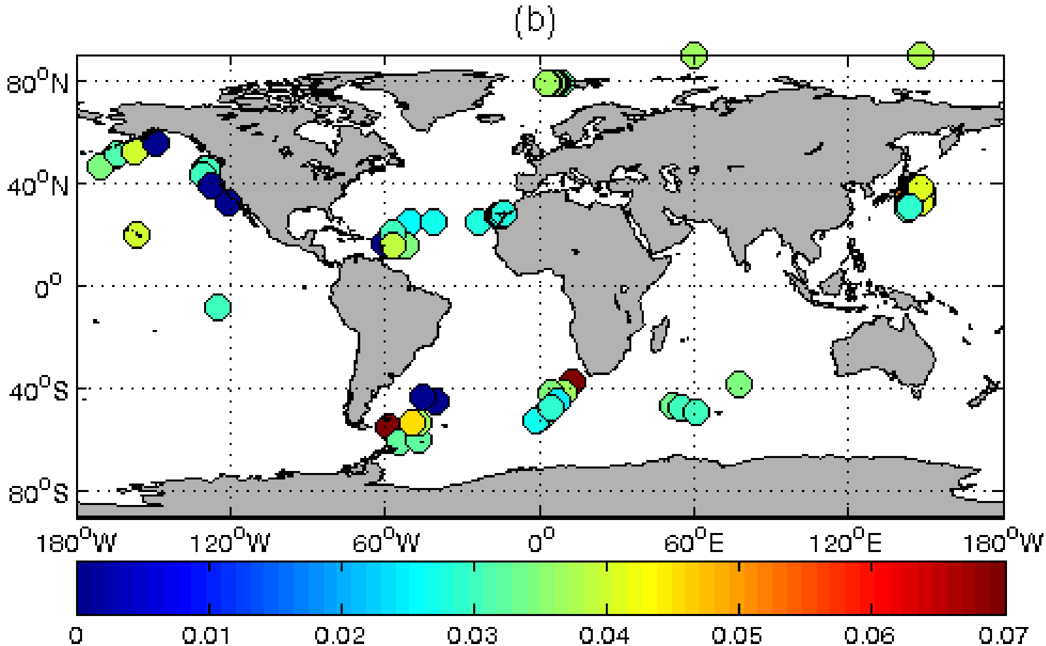
(b)
80°N
40°N
0°
40°S
80°S
180°W
120°W
60°W
0°
60°E
120°E
180°W
0
0.01
0.02
0.03
0.04
0.05
0.06
0.07

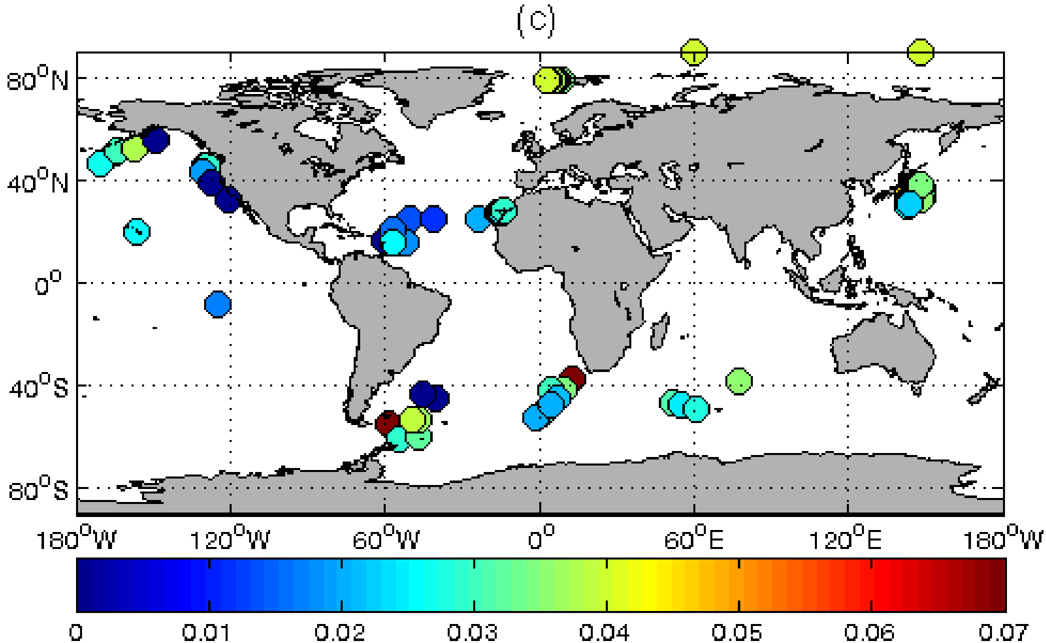
(c)
80°N
40°N
0°
40°S
80°S
180°W
120°W
60°W
0°
60°E
120°E
180°W
0
0.01
0.02
0.03
0.04
0.05
0.06
0.07

(d)

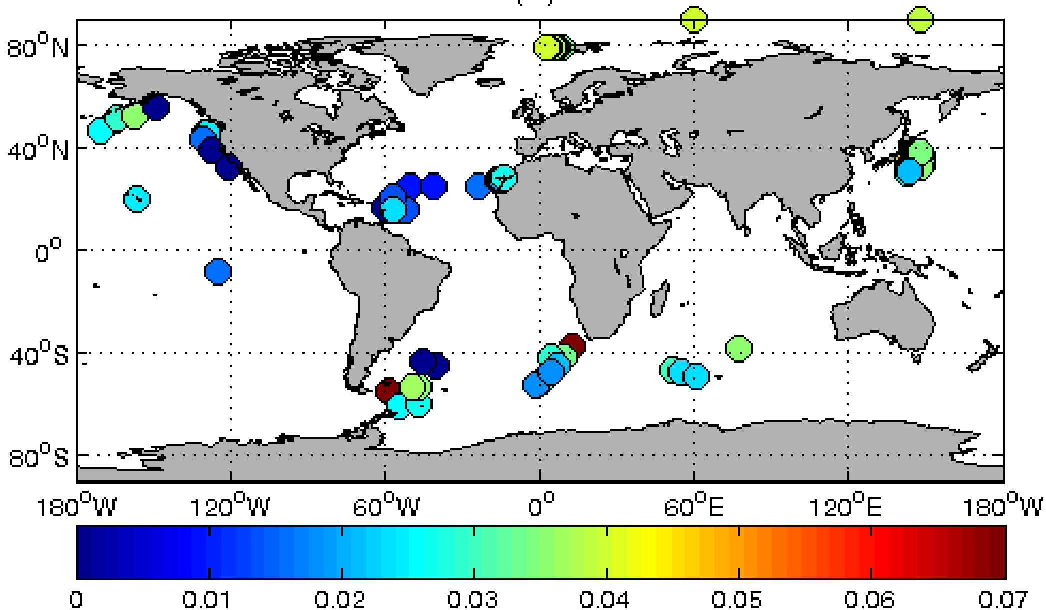

80°N
40°N
0°
40°S
80°S
180°W
120°W
60°W
0°
60°E
120°E
180°W
0
0.01
0.02
0.03
0.04
0.05
0.06
0.07

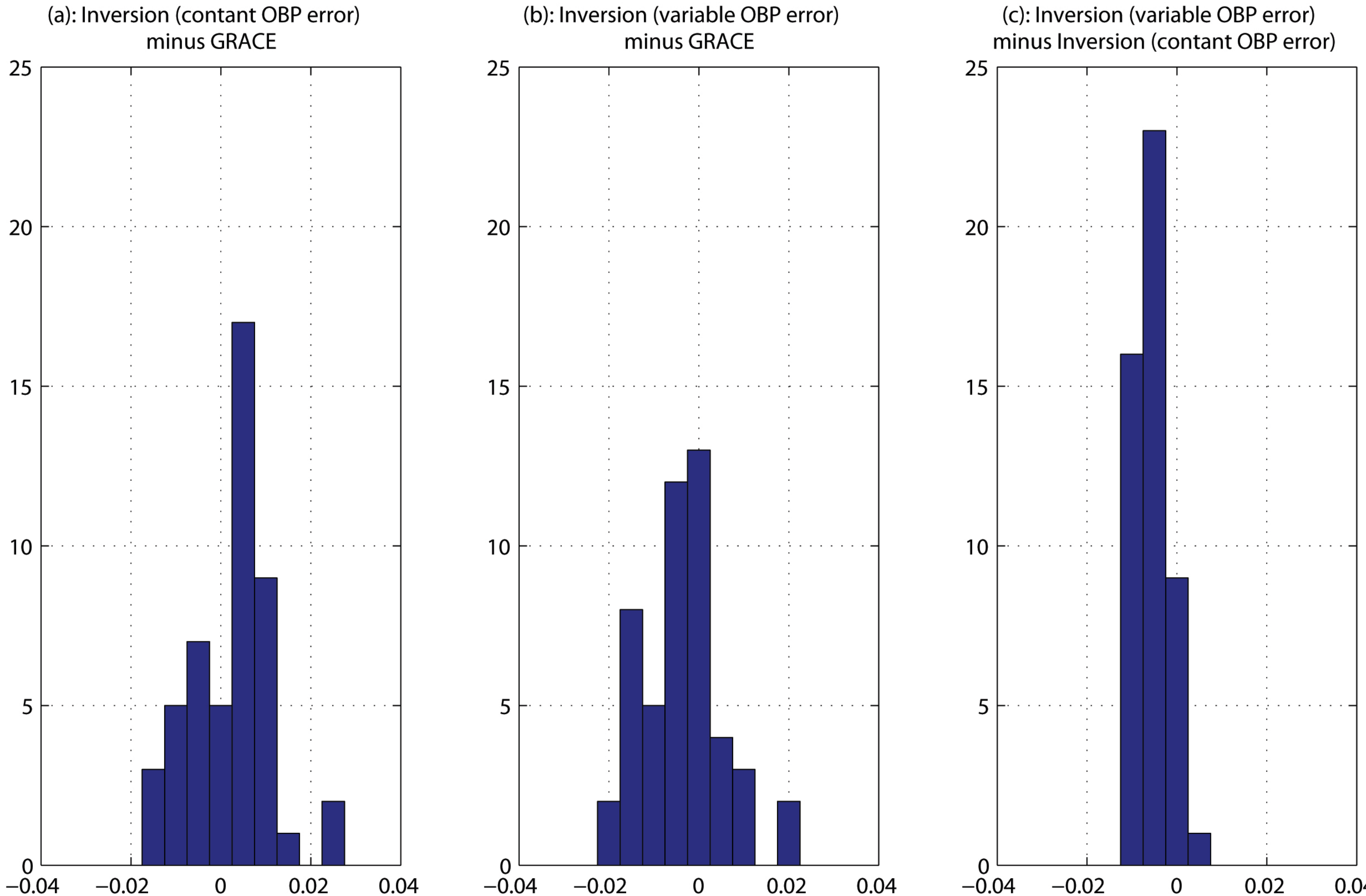
(a): Inversion (contant OBP error)
minus GRACE
(b): Inversion (variable OBP error)
minus GRACE
(c): Inversion (variable OBP error)
minus Inversion (contant OBP error)
0
5
10
15
20
25
−0.04
−0.02
0
0.02
0.04

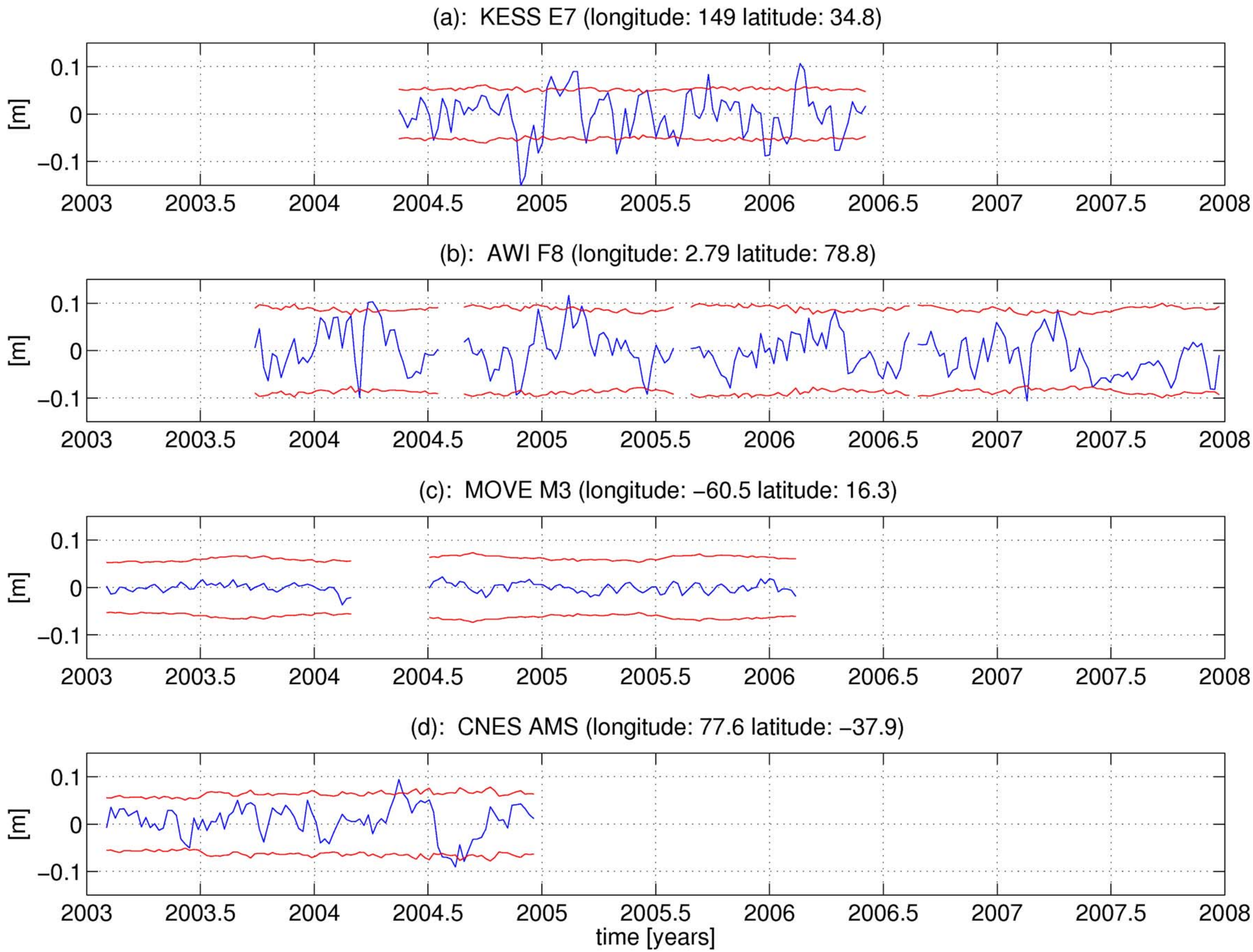

(a): KESS E7 (longitude: 149 latitude: 34.8)
(b): AWI F8 (longitude: 2.79 latitude: 78.8)
(c): MOVE M3 (longitude: −60.5 latitude: 16.3)
(d): CNES AMS (longitude: 77.6 latitude: −37.9)
[m]
0.1
0
−0.1
2003
2003.5
2004
2004.5
2005
2005.5
2006
2006.5
2007
2007.5
2008
time [years]